Japanese Journal of Radiology
https://doi.org/10.1007/s11604-018-0794-4

INVITED REVIEW

Machine learning studies on major brain diseases: 5-year trends of 2014–2018

Koji Sakai[1] · **Kei Yamada**[1]

Received: 21 October 2018 / Accepted: 14 November 2018
© Japan Radiological Society 2018

Abstract
In the recent 5 years (2014–2018), there has been growing interest in the use of machine learning (ML) techniques to explore image diagnosis and prognosis of therapeutic lesion changes within the area of neuroradiology. However, to date, the majority of research trend and current status have not been clearly illuminated in the neuroradiology field. More than 1000 papers have been published during the past 5 years on subject classification and prediction focused on multiple brain disorders. We provide a survey of 209 papers in this field with a focus on top ten active areas of research; i.e., Alzheimer's disease/mild cognitive impairment, brain tumor; schizophrenia, depressive disorders, Parkinson's disease, attention-deficit hyperactivity disorder, autism spectrum disease, epilepsy, multiple sclerosis, stroke, and traumatic brain injury. Detailed information of these studies, such as ML methods, sample size, type of inputted features and reported accuracy, are summarized. This paper reviews the evidences, current limitations and status of studies using ML to assess brain disorders in neuroimaging data. The main bottleneck of this research field is still the limited sample size, which could be potentially addressed by modern data sharing models, such as ADNI.

Keywords Artificial intelligence · Machine learning · Neurological disorder · Neuroimaging · Diagnosis

Introduction

Wang and Summers [1] predicted the future of machine learning (ML) in radiology and stated that "statistical approaches will be a major direction on ML study in radiology." They expected machine learning to be "a critical component of advanced software systems in the field of radiology." Conceptually their prediction is correct; however, up to the present day its practical application in radiology has not yet been proven to be entirely feasible. Limited sample size has been the largest issue hindering ML advancements in the field of radiology during the last 6 years. To achieve significant statistical power, large amounts of data are necessary. Wang and Summers' prediction on the statistical underlying basis of ML was correct; however, curious enough, the basis of their own hypothesis has been the major hindering factor for its development.

Does the "small *N*" problem [2] still have an adverse effect on ML study in the field of neuroradiology? Accordingly, has there been any recent progress on ML studies? In this review, we tried answering these questions by acquiring the ML research trend thorough literature search. We used keyword paper search on Pubmed [3].

In this article, we focused on the efficiency of ML techniques, with special focus on brain diseases. To capture the research trend from 2014 to 2018 (5 years), we picked up top ten active studies according to the number of papers (conference papers were excluded). These included Alzheimer's disease (AD)/mild cognitive impairment (MCI), brain tumor; schizophrenia (SCZ), depressive disorders, Parkinson's disease (PD), attention-deficit hyperactivity disorder (ADHD), autism spectrum disease (ASD), epilepsy, multiple sclerosis (MS), stroke, and traumatic brain injury (TBI). Detailed information about those studies such as ML methods, sample size, type of input features and reported accuracy were summarized. Based on this survey, we will try to clarify the current status and bottlenecks of ML studies.

✉ Koji Sakai
sakai3@koto.kpu-m.ac.jp

[1] Department of Radiology, Graduate School of Medical Science, Kyoto Prefectural University of Medicine, Kajii-cho, Kawaramachi Hirokoji Agaru, Kamigyo-ku, Kyoto, Kyoto 602-8566, Japan

Published online: 29 November 2018

Survey

Based on PubMed search from 2014 to 2018, 1337 papers on neuroimage-based ML researches were found. The key search terms: brain, machine learning, and diagnosis. Figure 1 summarizes the literature selection procedure for this paper.

An initial 1337 studies were identified using the search strategy described above, and 511 of these were screened by the title after removing the duplicates. A total of 467 abstracts were screened and 44 studies were excluded at this point. This left 340 studies screened by full-text, with 127 studies excluded at this juncture. We limited our search to journal papers in English, published up to 19 September 2018. In a few instances, the full paper was not found and therefore those studies were excluded from this survey. This review was conducted partially according to the Preferred Reporting Items for Systematic Reviews and Meta-Analyses (PRISMA) guidelines for systematic reviews [4].

Total of 209 papers were eventually selected based on the number of papers on top ten researches selected. The key aspects of each study, such as research purpose, machine learning method, imaging modality (ultrasonography was excluded), sample size, inputted features for ML, and remarks were investigated. Those that did not show results as numerical values were considered not eligible.

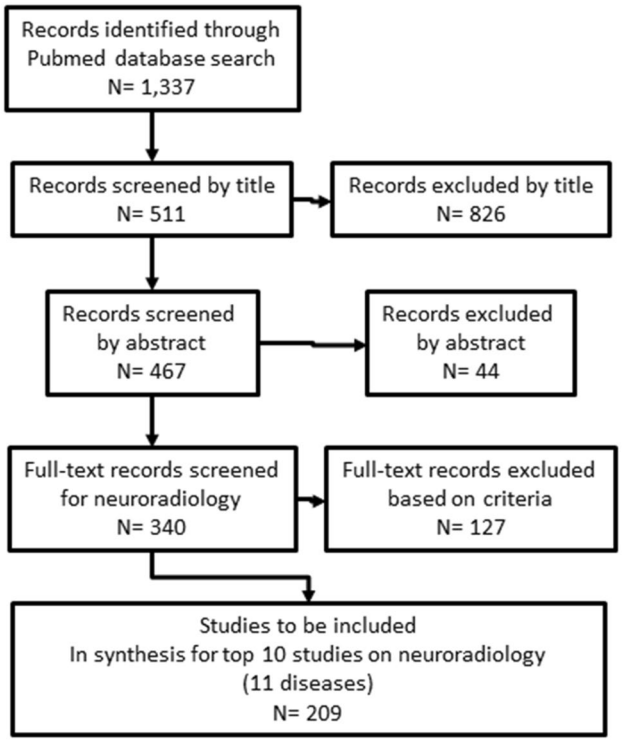

Fig. 1 Literature selection procedure

A list of all abbreviations used in the tables and the manuscript is provided in Table 1.

Results

Top ten studied brain diseases

Table 2 shows the top 10 studied brain diseases, their number of publications from 2014 to 2018, and relating large data sets. The top ten research areas for this survey were AD/MCI (62 papers), brain tumor (37 papers), schizophrenia (21 papers), depressive disorders (20 papers), PD (13 papers), ADHD (13 papers), ASD (12 papers), epilepsy (10 papers), MS (8 papers), stroke (7 papers), and TBI (7 papers).

Alzheimer's disease/mild cognitive impairment

MCI is considered a prodromal phase to dementia, especially the AD type. AD is the most common neurodegenerative disorder, which is increasingly prevalent among adults aged 65 years and older. Considering the prevalence and severity of MCI/AD, the largest number of neuroimaging-based, automatic classification publications has been published. Also, a number of these studies investigated the possibility of automatic classification of stable MCI (sMCI) from progressive MCI (pMCI) and converter MCI from non-converter MCI using ML plus neuroimaging. Table 3 summarizes the 55 papers. 48 papers (83%) among 55 were studied about classification of AD, MCI (including subtypes), and normal controls.

Brain tumor

A central goal of ML on brain tumor is the identification of quantitative imaging indicators that predict important clinical outcomes, including prognosis and response or resistance to a specific cancer treatment [65]. The main purposes of the surveyed ML studies on brain tumor were segmentation of the tumor, classification of the type of tumor, and prediction of survival or genotype. MRI was the main modality for ML studies. Depending on the purpose, variety of MR imaging methods were employed. Table 4 summarizes the brain tumor studies.

Schizophrenia

Considering the absence of standard clinical test for schizophrenia, there is a growing interest in automatic diagnosis of schizophrenia based on neuroimaging features [2]. Therefore, all studies aimed to identify and classify SCZ from healthy control and/or other psychiatric diseases such

Table 1 Abbreviations used in the tables and manuscript

Abbreviation	Full term
(a) Used in informatics	
3D HOG	Histogram of oriented 3D gradients
BIRN	The Biomedical Informatics Research Network
CRF	Conditional random fields
CV	Cross validation
DANS	Discriminant autoencoder network with sparsity constraint
DBM	Deep Boltzmann machine
DBN	Deep belief network
DDN	Deep delief network
DESRN	Deep ensemble sparse regression network
DF	Deformation fields
DLDA	Diagonal linear discriminate analysis
DNN	Deep neural network
DQDA	Diagonal quadratic discriminate analysis
DRBMs	Discriminative restricted Boltzmann machines
ELM	Extreme learning machines
EPNN	Enhanced probabilistic neural network
FASMA	Fast spectroscopic multiple analysis
FCM	Fuzzy C-means
FWT	Fast wavelet decomposition
GMLVQ	Generalized matrix learning vector quantization
GNB	Gaussian Naïve Bayes
IFWT	Fast wavelet reconstruction
IPSO	Improved particle swarm optimization
IVM	Import vector machine
JFSS	Joint feature-sample selection
k-NN	*k*-Nearest neighbor
KSOM	Kohonen self-organizing map
KPLS	Kernel partial least squares regression
LASSO	Least absolute shrinkage and selection operator
LDA	Linear discriminant analysis
LDS	Low density separation
LG	Label generation
LINDA	Lesion identification with neighborhood data analysis
LOOCV	Leave-one-out cross validation
LOSPGOCV	Leave-one-subject-per-group-out cross validation
LOSOCV	Leave-one-subject-out cross validation
LPOCV	Leave-pair-out cross validation
LSOCV	Leave-site-out cross validation
LTOCV	Leave-two-out cross validation
LR	Logistic regression
LR	Logistic regression
M2TL	Multimodal manifold-regularized transfer learning
MCCV	Monte carlo cross-validation
MIMC	Multi-label inductive matrix completion
ML	Machine learning
MLDA	Maximum entropy linear discriminant analysis
MMC	Maximum margin clustering
MPA	Multivoxel pattern analyses
MVPA	Multi-voxel pattern analysis

Table 1 (continued)

Abbreviation	Full term
NMF	Non-negative matrix factorization
NN	Neural Network
OASIS	Open access series of imaging studies
OC-SVM	One-class support vector machine.
OOB	Out-of-bag
OVA	One-versus-all
PNN	Robabilistic neural network
RBF	Radial based function
RBM	Restricted Boltzmann machine
RDF	Random decision forest
RELM	Regularized extreme learning machine
RF	Random forest
RFE	Recursive feature elimination
RLDA	Robust discriminant analysis
SBFE	Searchlight based feature extraction
SLFN	Single layer feedforward networks
SMSMA	Supervised multiblock sparse multivariable analysis
SVM	Support vector machine
SWCSD	Supervised within-class-similar discriminative
TGSL	Temporally-constrained group sparse learning
(b) Used in medicine	
11C-MET	L-[Methyl-11C methionine
FP-CIT SPECT	123Iodine-labelled *N*-(3-fluoropropyl)-2β-carbomethoxy-3β-(4-iodophenyl) nortropane (123I-FP-CIT) single photon emission computerized tomography
AD	Alzheimer's disease
ADC	Apparent diffusion coefficient
ADNI	Alzheimer's disease Neuroimaging Initiative
AH	Auditory hallucinations
AIBL	The Australian Imaging, Biomarker and Lifestyle Flagship Study of Ageing
ASD	Autism spectrum disease
AUC	Area under the curve
BD	Bipolar disorder
BIRN	The Biomedical Informatics Research Network
BRATS	Multimodal Brain Tumor Segmentation Challenge
CL	Cognitive loss
CLIMB	The Comprehensive Longitudinal Investigation of MS at the Brigham and Women's Hospital Partners MS Center
cMDD	Current major depressive disorder patients
CMRGlc	Cerebral metabolic rate of glucose consumption
COBRE	The Center for Biomedical Research Excellence
CSF	Cerebrospinal fluid
CT	Computed tomography
cT1WI	Contrast enhanced T1WI
DBS	Deep brain stimulation
DKI	Diffusion kurtosis image
dMRI	Diffusion MRI
DSM	Diagnosis and Statistical Manual of Mental Disorders
DTI	Diffusion tensor image
DZNE	The German center for neurodegenerative diseases
ECT	Electroconvulsive therapy
EEG	Electroencephalogram

Table 1 (continued)

Abbreviation	Full term
EP	Ependymoma
FA	Fractional anisotropy
FDG-PET	2-Deoxy-2-[18F]fluoroglucose PET
FLAIR	Fluid attenuated inversion recovery
fMRI	Functional MRI
GBM	Glioblastoma multiforme
GM	Gray matter
HARDI	High angular resolution diffusion images
HC	Healthy control
HNPPH	Henan provincial people's hospital
HR	High risk
LBP	Local binary pattern
LGG	low grade glioma
MB	Medulloblastoma
MBs	Medulloblastomas
MCI	Mild cognitive impairment
MCI-C	MCI converter
MCI-NC	MCI non-converter
MD	Mean diffusivity
MDD	Major depressive disorder
MEG	Magnetoencephalography
MEN	Meningioma
MI	Motor function impaired
MP	Motor function preserved
MPRAGE	Magnetization-prepared rapid acquisition with gradient echo
MR	Magnetic resonance
MRI	Magnetic resonance image
MS	Multiple sclerosis
mTBI	Mild traumatic brain injury
MTS	Mesial temporal sclerosis
NC	Normal control
NIH	National Institutes of Health
NITRC	The Neuroimaging Informatics Tools and Resources Clearinghouse
OASIS	The Open Access Series of Imaging Studies
OCD	Obsessive compulsive disorder
PAs	Pilocytic astrocytomas
PCS	Post concussion syndrome
PD	Parkinson's disease
PDWI	Proton density weighted image
PET	Photon emission tomography
PiB	Pittsburg compound B
pMCI	Progressive MCI
PPI	Psychophysiological interaction
PPMI	Parkinson's progression markers initiative
PRODEM	The prospective registry on dementia
PSP	Progressive supranuclear palsy
PTSD	Posttraumatic stress disorder
R2*WI	R2* weighted image
rMDD	Remitted major depressive disorder patients
RNA	Ribonucleic acid

Table 1 (continued)

Abbreviation	Full term
rCBV	Relative cerebral blood volume
rRCBV	Relative regional cerebral blood volume
rs-fMRI	Resting state fMRI
sMCI	Stable MCI
sMRI	Structural MRI
SCI	Subjective cognitive impairment
SCZ	Schizophrenia
SIB	Non-affected siblings of patients with schizophrenia
SICH	Symptomatic intracranial haemorrhage
sMRI	Structural MRI
SNP	Single nucleotide polymorphism
SUVr	Standard uptake value ratio
SWEDD	Subjects with scans without evidence of dopaminergic deficit
T1WI	T1 weighted image
T2WI	T2 weighted image
TBI	Traumatic brain injury
TCGA	The cancer genome atlas
TCIA	The cancer imaging archive
WM	White matter

Table 2 Top ten studied brain diseases, their number of publications from 2014 to 2018, and related large data sets

Rank	Disease	Number of papers	Large data set based studies	Large data set
1	Alzheimer's disease/MCI	61	51 (83.6%)	ADNI, OASIS, DZNE, PRODEM, AIBL
2	Brain tumor	37	6 (16.2%)	BRATS, TCIA, TCGA
3	Schizophrenia	21	4 (19.0%)	COBRE, NITRC, BIRN
4	Depression	20	0 (0.0%)	–
5	Parkinson's disease	13	9 (69.2%)	PPMI
5	ADHD	13	8 (61.5%)	ADHD-200[a], ABIDE[b]
7	Autism	12	10 (83.3%)	ABIDE[b]
8	Epilepsy	10	0 (0.0%)	–
9	Multiple sclerosis	8	1 (12.5%)	CLIMB
10	Stroke	7	0 (0.0%)	–
10	Traumatic brain injury	7	0 (0.0%)	–
	Sum	209	89 (43.8%)	

[a]ADHD-200: http://fcon_1000.projects.nitrc.org/indi/adhd200/

[b]ABIDE: http://fcon_1000.projects.nitrc.org/indi/abide/databases.html

as bipolar disorder [106] or OCD [104]. We surveyed 21 papers, which are presented in Table 5.

Depressive disorders

The diagnosis of major depression disorders (MDD) is based on application of criteria from the Diagnosis and Statistical Manual of Mental Disorders (DSM) and clinician judgment. Based on the diagnosis, initial pharmacotherapy treatment is effective in approximately 50% of patients [124]. Therefore, the main purposes of ML studies on MDD were classification and prediction of the first onset [140], treatment response [142, 143], and clinical depression score [144]. We reviewed 19 studies that used neuroimaging for automatic diagnoses of MDD. Those studies are listed in Table 6.

Table 3 Summary of AD/MCI studies

Purpose	Disorder	Modality	Feature	Classifier	Validation	Overall accuracy	Number of subjects	Data base[a]	Author	Year	References
Classification	MCI	rs-fMRI	Functional connectivity network	SVM	LOOCV	0.919 (MCI vs NC)	MCI = 12, NC = 25, total = 37	Internal	Jie et al.	2014	[5]
Classification	AD/MCI	sMRI	Local binary pattern	SVM	10-fold CV	0.828 (AD vs HC), 0.615 (MCI vs NC)	AD = 80, pMCI = 141, HC = 142, total = 363	ADNI	Li et al.	2014	[6]
Classification	AD	sMRI, DTI	DTI features	SVM	LOOCV	0.943 (AD vs HC),	AD = 21, HC = 15, total = 36	Internal	Li et al.	2014	[7]
Classification	MCI	sMRI	Cortical features	SVM	LOOCV	0.8 (aMCI vs NC)	aMCI = 24, NC = 26, total = 50	Internal	Li et al.	2014	[8]
Classification	AD/MCI	T1WI	Voxel-wise imaging features	SVM	10-fold CV	0.9 (AD vs HC), 0.87 (pMCI vs NC), 0.71 (pMCIvs sMCI)	AD = 198, pMCI = 167, sMCI = 236, HC = 229, total = 830	ADNI	Liu et al.	2014	[9]
Classification	MCI	PET	Neuropsychological test data	SVM	N/A	0.89 (cMCI vs sMCI)	cMCI = 25, sMCI = 20, total = 45	Internal	Segovia et al.	2014	[10]
Classification	AD/MCI	sMRI, FDG-PET	GM structure, PET, CSF biomarker	SVM	10-fold CV	0.95 (AD vs HC), 0.8 (MCI vs NC), 0.746 (MCI vs AD), 0.72 (ncMCI vs cMCI)	AD = 51, cMCI = 43, ncMCI = 56, HC = 52, total = 202	ADNI	Suk et al.	2014	[11]
Classification	MCI	MRI, PET	189 features (93 MRI, 93PET, 3 CSF)	M2TL	10-fold CV	0.801 (cMCI vs ncMCI)	AD = 51, cMCI = 43, ncMCI = 56, NC = 52, total = 202	ADNI	Cheng et al.	2015	[12]
Classification	AD	dMRI, rs-fMRI, sMRI	Fiber tract integrity, graph-theoretical measures, GM volume	SVM	LOOCV	0.85 (AD vs HC)	AD = 28, HC = 25, total = 53	DZNE	Dyrba et al.	2015	[13]
Classification	AD	MRI	Longitudinal percentage of brain volume changes	SVM + RBF	k-fold CV	0.917 (AD vs HC)	AD = 30, HC = 30, total = 60	ADNI	Farzan et al.	2015	[14]

Table 3 (continued)

Purpose	Disorder	Modality	Feature	Classifier	Validation	Overall accuracy	Number of subjects	Data base[a]	Author	Year	References
Classification	AD/MCI	MRI, FDG-PET	GM volume, average intensity of PET	SVM	10-fold CV	0.9503 (AD vs HC), 0.7927 (MCI vs NC), 0.689 (cMCI vs ncMCI)	AD = 51, pMCI = 99, HC = 52, total = 202	ADNI	Jie et al.	2015	[15]
Classification	AD	rs-fMRI	Network-based features	SVM	LOOCV	1.0 (AD vs HC)	AD = 20, HC = 20, total = 40	ADNI	Khazaee et al.	2015	[16]
Classification	AD/MCI	MRI	GM volumetric features	SVM	10-fold CV	0.925 (AD vs HC), 0.79 (pMCIvs sMCI)	AD = 97, pMCI = 117, sMCI = 117, HC = 128, total = 459	ADNI	Liu et al.	2015	[17]
Classification	AD/MCI	MRI, PET	GM volume, regional ave. CMRGlc	SVM	10-fold CV	0.91 (AD vs HC), 0.82 (MCI vs NC)	AD = 85, cMCI = 67, ncMCI = 102, HC = 77, total = 331	ADNI	Liu et al.	2015	[18]
Classification	AD	MPRAGE	Smoothed GM density values	SVM, LDS	2 nested CV loops	0.74 (AD vs NC)	AD = 200, pMCI = 164, sMCI = 100, HC = 231, total = 695	ADNI	Moradi et al.	2015	[19]
Classification	AD/MCI	MRI, FDG-PET, florbetapir PET	GM volume, SUVr	wmSRC	N/A	0.948 (AD vs HC), 0.745 (MCI vs HC), 0.778 (pMCIvs sMCI)	AD = 113, pMCI = 110, HC = 117, total = 340	ADNI	Xu et al.	2015	[20]
Classification	AD/MCI	MRI, PET	HOG	SVM	10-fold CV	0.913 (AD vs HC), 0.781 (MCI vs HC), 0.755 (pMCI vs sMCI)	AD = 198, pMCI = 124, sMCI = 118, HC = 229, total = 669	ADNI	Zhu et al.	2015	[21]
Classification	AD	11C-PiB PET	3D HOG, amyloid status	SVM	LOOCV	1.00 (AD vs HC)	AD = 167, HC = 42, total = 209	ADNI	Cattell et al.	2016	[22]
Classification	AD/MCI	PET, rs-fMRI	Feature graph	SVM	LOOCV	0.9714 (AD vs HC), 0.9 (MCI vs NC)	AD = 30, EMCI = 30, HC = 60, total = 120	ADNI	Hu et al.	2016	[23]

Table 3 (continued)

Purpose	Disorder	Modality	Feature	Classifier	Validation	Overall accuracy	Number of subjects	Data base[a]	Author	Year	References
Classification	AD/MCI	rs-fMRI	Graph measures	SVM	23-fold CV	0.873 (NC vs AD/MCI), 0.975 (AD vs NC/MCI), 0.72 (MCI vs NC/AD)	AD = 34, MCI = 89, NC = 45, total = 168	ADNI	Khazaee et al.	2016	[24]
Classification	AD/MCI	T1WI	GM density map	SVM	10-fold CV	0.9306 (AD vs HC), 0.7925 (pMCI vs sMCI)	AD = 97, pMCI = 117, sMCI = 117, HC = 128, total = 459	ADNI	Liu et al.	2016	[25]
Classification	AD	rs-fMRI	rs-fMRI feature	SVM	LOOCV	0.76 (AD vs HC)	AD = 25, HC = 34, total = 59	ADNI	Ni et al.	2016	[26]
Classification	MCI	rs-fMRI	Functional connectivity	RBM	LOOCV	0.7258 (MCI vs NC)	MCI = 31, NC = 31, total = 62	ADNI2	Suk et al.	2016	[27]
Classification	AD/MCI	MRI, PET	Feature graph	SVM	10-fold CV	0.926 (AD vs HC), 0.8 (MCI vs NC)	AD = 50, pMCI = 97, HC = 52, total = 199	ADNI	Yu et al.	2016	[28]
Classification	AD/MCI	MRI, FDG-PET	GM volume, average intensity of PET	SVM	10-fold CV	0.9595 (AD vs HC), 0.8026 (MCI vs NC)	AD = 51, pMCI = 99, HC = 52, total = 202	ADNI	Zu et al.	2016	[29]
Classification	AD/MCI	sMRI	MRI, SNP features	SVM	N/A	0.92 (AD vs HC), 0.8 (MCI vs HC), 0.81 (pMCI vs sMCI)	AD = 171, pMCI = 157, sMCI = 205, HC = 204, total = 737	ADNI	An et al.	2017	[30]
Classification	MCI	T1WI	GM region atrophy	SVM	10-fold CV	0.93 (pMCI vs sMCI)	AD = 92, pMCI = 70, sMCI = 65, HC = 94, total = 321	ADNI	Beheshti et al.	2017	[31]
Classification	MCI	rs-fMRI, DTI	Functional connectivity	SVM	LOOCV	0.787 (MCI vs NC)	MCI = 54, NC = 54, total = 108	ADNI	Chen et al.	2017	[32]

Table 3 (continued)

Purpose	Disorder	Modality	Feature	Classifier	Validation	Overall accuracy	Number of subjects	Data base[a]	Author	Year	References
Classification	AD	T1WI	GM density map	LASSO	10-fold CV	0.81 (AD vs HC)	AD = 137, SCI = 38, MCI = 78, HC = 355, total = 608	ADNI	Doan et al.	2017	[33]
Classification	AD	MRI, PET	5 ROI, 6 shape, 2 volume features	SVM	CV	0.8813 (MCI vs NC)	AD = 137, cMCI = 76, HC = 162, total = 375	ADNI	Glozman et al.	2017	[34]
Classification	MCI	MRI	Cortical surface based measurements	SVM	Stratified shuffle split CV	0.77 (naMCI vs aMCI), 0.81 (aMCI vs CN), 0.7 (naMCI vs CN)	aMCI = 40, naMCI = 27, NC = 117, total = 184	Internal	Guan et al.	2017	[35]
Classification	AD	rs-fMRI	Connectivity hyper-networks	SVM	10-fold CV	0.916 (AD vs HC)	AD = 38, HC = 28, total = 66	Internal	Guo et al.	2017	[36]
Classification	MCI	rs-fMRI	Graph measures	SVM	LOOCV, 9-fold CV	0.914	cMCI = 18, ncMCI = 62, total = 80	ADNI	Hojjati et al.	2017	[37]
Classification	AD	T1WI, PET	GM volume, average intensity of PET	SMSMA	10-fold CV	AUC = 0.95	AD = 52, HC = 48, total = 100	ADNI	Kawaguchi et al.	2017	[38]
Classification	AD/MCI	rs-fMRI	Graph measures	Naïve Bayes	10-fold CV	0.9329 (MCI vs AD)	AD = 34, MCI = 89, NC =45, total = 168	ADNI	Khazaee et al.	2017	[39]
Classification	AD	MRI, PET	Structural measures	SVM, IVM, RELM	70/30 CV, 10-fold CV, LOOCV	0.7788 (AD vs HC),	AD = 70, pMCI = 74, HC = 70, total = 214	ADNI	Lama et al.	2017	[40]
Classification	AD/MCI	sMRI, FDG-PET, florbetapir PET	Mean GM volume, SUVr	SCDDL	10-fold CV	0.9736 (AD vs HC), 0.7766 (MCI vs HC)	AD = 113, pMCI = 110, HC = 117, total = 340	ADNI	Li et al.	2017	[41]
Classification	AD/MCI	MRI	GM, amygdara	SVM	10-fold CV	0.965 (AD vs HC), 0.9174 (pMCI vs HC), 0.8899 (pMCI vs sMCI)	AD = 65, pMCI = 95, sMCI = 132, HC = 135, total = 427	ADNI	Long et al.	2017	[42]

Table 3 (continued)

Purpose	Disorder	Modality	Feature	Classifier	Validation	Overall accuracy	Number of subjects	Data base[a]	Author	Year	References
Classification	AD	T1WI	Regional volume	Automated volumetric assessment tool	N/A	1.00 (AD vs HC)	AD = 30, HC = 25, total = 55	Internal	Min et al.	2017	[43]
Classification	AD	MRI, blood lipid	Lipidomics	Random forest	Training/test (2/1)	0.71(AD vs HC)	AD = 142, HC = 135, total = 277	Internal	Proitsi et al.	2017	[44]
Classification	AD/MCI	sMRI	Cortical thickness, hippocampal shape, hippocampal texture, and volumetry	LDA	10-fold CV	0.969 (NC vs AD/MCI), 0.612 (AD vs NC/MCI), 0.287 (MCI vs NC/AD)	N/A	The CAD-Dementia challenge	Sørensen et al.	2017	[45]
Classification	AD/MCI	sMRI	Spatially normalized GM densities	Deep ESR net	10-fold CV	0.91 (AD vs HC), 0.73 (MCI vs NC), 0.748 (pMCIvs sMCI)	AD = 186, pMCI = 167, sMCI = 226, HC = 226, total = 805	ADNI	Suk et al.	2017	[46]
Classification	AD/MCI	MPRAGE, PiB-PET	GM volume, intensity of PET	Simple MKL	10-fold CV	0.957 (AD vs HC), 0.958 (MCI vs NC), 0.951 (MCI vs AD)	AD = 52, pMCI = 108, HC = 120, total = 280	AIBL	Youssofzadeh et al.	2017	[47]
Classification	AD/MCI	MRI	GM volume	SVM	10-fold CV	0.903 (AD vs HC), 0.722 (MCI vs NC), 0.713 (sMCI vs cMCI)	AD = 186, pMCI = 393, HC = 226, total = 805	ADNI	Zhu et al.	2017	[48]
Classification	AD/MCI	MRI, PET	GM volume, intensity of PET	SVM	10-fold CV	0.957 (AD vs HC), 0.799 (MCI vs HC), 0.724 (ncMCI vs cMCI)	AD = 51, cMCI = 143, ncMCI = 156, HC = 52, total = 402	ADNI	Zhu et al.	2017	[49]
Classification	AD	MRI	Hippocampal	HUMAN	N/A	0.20 (AD vs NC)	AD = 132, pMCI = 250, HC = 174, total = 556	ADNI	Amoroso et al.	2018	[50]
Classification	AD	FDG-PET, florbetapir PET	PET images	Deep CNN	10-fold CV	0.96 (AD vs HC)	AD = 139, pMCI = 79, sMCI = 92, HC = 182, total = 492	ADNI-2	Choi et al.	2018	[51]

Table 3 (continued)

Purpose	Disorder	Modality	Feature	Classifier	Validation	Overall accuracy	Number of subjects	Data base[a]	Author	Year	References
Classification	AD	FDG-PET	Intensity of PET	SVM	LOOCV	0.9788 (AD vs HC)	AD = 81, pMCI = 29, HC = 61, total = 171	Internal	Garali et al.	2018	[52]
Classification	AD/MCI	MRI, FDG-PET	Volume, mean intensity, CSF features (p-tau, t-tau, Aβ42)	ELM	10-fold CV	0.971 (AD vs HC), 0.871 (MCI vs HC)	AD = 51, pMCI = 99, HC = 52, total = 202	ADNI	Kim et al.	2018	[53]
Classification	AD/MCI	T1WI, FDG-PET	3D image patch	CNN	10-fold CV	0.933 (AD vs HC), 0.83 (sMCI vs NC), 0.64 (pMCI vs NC)	AD = 93, pMCI = 204, HC = 100, total = 397	ADNI	Liu et al.	2018	[54]
Classification	AD	MRI, PET, SPECT	FDG-PET	SVM	LOOCV	0.93 (AD vs HC)	AD = 20, HC = 18, total = 38	Internal	Rondina et al.	2018	[55]
Classification	AD/MCI	MRI	Kaggle-neuroimaging-challenge: 429 features (demographic, clinical features)	SVM	5-fold CV	0.96 (AD vs HC), 0.9 (cMCI vs AD), 0.78 (ncMCI vs AD), 0.62 (ncMCI vs cMCI), 0.79 (cMCI vs HC), 0.59 (ncMCI vs HC)	AD = 44, cMCI = 44, ncMCI = 44, HC = 44, total = 176	ADNI	Salvatore et al.	2018	[56]
Classification	AD/MCI	MRI	GM density map	SVM	Training/test (1/1)	0.928 (AD vs HC), 0.708 (MCI vs NC), 0.64 (sMCI vs cMCI), 0.657 (MCI vs AD)	AD = 186, cMCI = 167, sMCI = 226, HC = 226, total = 805	ADNI	Sun et al.	2018	[57]
Classification	AD	MPRAGE	Image intensity	CNN	Training/test (1/1)	0.977 (AD vs HC)	AD = 98, HC = 98, total = 196	OASIS, internal	Wang et al.	2018	[58]
Detection	AD	DTI, DKI	DTI, DKI measures	SVM	LOOCV	0.96 (AD vs HC)	AD = 27, HC = 26, total = 53	Internal	Chen et al.	2017	[59]
Diagnosis	AD	DTI	FA-ICA	Elastc net	10-fold CV	0.85 (AD vs HC)	AD = 77, HC = 173, total = 250	PRODEM	Schouten et al.	2017	[60]

Table 3 (continued)

Purpose	Disorder	Modality	Feature	Classifier	Validation	Overall accuracy	Number of subjects	Data base[a]	Author	Year	References
Diagnosis	AD	MRI, FDG-PET	Hippocampal texture	SVM	20-fold CV	AUC = 0.74/0.83 (MCI to AD)	AD = 101, pMCI = 233, HC = 169, total = 503/ AD = 28, pMCI = 25, HC = 88, total = = 141	ADNI/AIBL	Sørensen et al.	2016	[61]
Diagnosis	AD	MRI, PET	HYDRA	SVM	10-fold CV	AUC = 0.91	AD = 123, HC = 177, total = 300	ADNI	Varol et al.	2017	[62]
Identification	AD	MRI	Morphological measures	Naïve Bayes, logistic regression, SVM	MCCV	0.85 (AD vs HC)	AD = 75, HC = 75, total = 150	OASIS	Cai et al.	2017	[63]
Prediction	AD/MCI	FDG-PET, florbetapir PET	PET images	Deep CNN	10-fold CV	0.84 (AD converter)	AD = 139, pMCI = 79, sMCI = 92, HC = 182, total = 492	ADNI-2	Choi et al.	2018	[64]
Prediction	AD	MRI	Total GM volume	tgLASSO	10-fold CV	0.757 (AD converter)	AD = 91, cMCI = 104, ncMCI = 98, HC = 152, total = 445	ADNI	Jie et al.	2017	[65]

N/A indicates information was not available or could not be found

[a]Internal: subjects were recruited from institutional and/or public through media channels

Table 4 Summary of brain tumor studies

Purpose	Type	Modality	Feature	Classifier	Validation	Accuracy	Number of subjects	Data base[a]	Author	Year	References
Detection	Glioma progression	(18)F-FDG PET, MRS	SUVmax, Cho conc., Cr conc.	SVM	LOOCV	0.83	Total = 12 (6II, 6III)	Internal	Imani et al.	2014	[66]
Segmentation	Brain tumor	T1WI, MRS	3D texture	ELM-IPSO	LOOCV	0.9915	Training = 35 (12 meningiomas, 23 gliomas)	Internal	Nachimuthu et al.	2014	[67]
Detection	Brain metastasis	T1WI, T2WI, FLAIR	Histogram, morphology, texture	Template-matching, k-means cluster, ANN	Training/test (80/60)	AUC = 0.874	Training = 80 (450 BM nodules), Test = 30 (134BM nodules), 30 (without nodules), Total = 140	Internal	Sunwoo et al.	2017	[68]
Segmentation	Tumor compartment	T1WI, cT1WI, T2WI, FLAIR	Superpixel	SVM	2-fold CV	0.975	Total = 20 GBM	BRATS2012	Wu et al.	2014	[69]
Segmentation	Tumor compartment, GBM	T2WI, DWI, PWI	T2WI, ADC, rCBV maps	FCM	N/A	0.84 - 0.92	Total = 13 GBM	Internal	Fathi et al.	2015	[70]
Segmentation	Tumor compartment	T1WI, cT1WIFLAIR, PWI	rRCBV, sveral ROIs	KFCM	N/A	0.7183	Total = 20 (9GBM, 4HG, 1DA, 5MEN, 1MET)	Internal	Szwarc et al.	2015	[71]
Segmentation	Brain tumor	T1WI, T1WIC, T2WI, FLAIR	Shape, size, contrast	DNN	Training/test (30/10)	0.88	Training = 30 (20 high grade, 10 low grade), test = 10 (high grade), Total = 40	BRATS2013	Havaei et al.	2017	[72]
Segmentation	LGG	T2WI, MRS	Image intensity, 11 metabolites feature vector	IFWT	LOOCV	0.9	Total = 7 LGG	Internal	Li et al.	2017	[73]
Segmentation	Tumor compartment	T1WI, cT1WI, FLAIR, PWI, DWI	6 contrasts	NMF	N/A	0.8	Total = 21 HGG	Internal	Sauwen et al.	2017	[74]
Segmentation	Brain tumor	MRI, FALIR	Contrast	CNN	10-fold CV	0.76	Total = 44 GBM	Internal	AlBadawy et al.	2018	[75]
Segmentation	Tumor compartment, glioma	18F-FET PET	PET image	3D U-net CNN	Training/test (26/11)	0.8231	Training = 26, Test = 11, Total = 37	Internal	Blanc-Durand et al.	2018	[76]
Segmentation	Tumor compartment	DTI	3D supervoxel	RF	N/A	0.89	Total = 30 (20 high grade, 10 low grade)	BRATS2013	Soltaninejad et al.	2018	[77]

Table 4 (continued)

Purpose	Type	Modality	Feature	Classifier	Validation	Accuracy	Number of subjects	Data base[a]	Author	Year	References
Segmentation	LGG, Glioma	T1WI, T2WI, FLAIR, cT1WI	Image intensity	CRF	N/A	0.823 (LGG), 0.823 (HGG)	Total = 54 LGG, 200 HGG, Test = 161, Total = 215	BRATS2013, 2015,HNPPH	Zhao et al.	2018	[78]
Classification	High vs low grade	T1WI, T2WI, DTI	Metrics	SVM	LOOCV	0.80	Total = 33 (14 LGG, 19HGG)	Internal	Inano et al.	2014	[79]
Classification	Brain tumor	T1WI, T2WI	3D texture	ANN	LOOCV	0.92	Total = 44 (21 MB, 20 PA, 7 EP)	Internal	Fetit et al.	2015	[80]
Classification	Glioblastoma	T1WI, T2WI, PWI, DTI	Texture features	DLDA, SQDA, SVM	Training/test (11/7)	0.82	Training = 11 (60 biopsies), test = 7 (22biopsies), Total = 18	Internal	Hu et al.	2015	[81]
Classification	Brain tumor	MRI, MRS,DWI, DTI, PWI	Computed metrics	SVM	10-fold CV	0.89	Total = 126	Internal	Tsolaki et al.	2015	[82]
Classification	Glioma	MRI	LBP features	Binary logistic regression	LOOCV	0.93	Total = 107 (73 LGG, 34 GBM)	TCIA	Li-Chun et al.	2017	[83]
Classification	Glioma	MRI	Histogram, texture feature	SVM, IBK	LOOCV	0.945 (high vs low grade), 0.961(II/III/IV)	Total = 120 (28LGG, 92HGG)	Internal	Zhang et al.	2017	[84]
Classification/ Prediction	Brain tumor, glioma	T1WI, T2WI, FLAIR, DWI	Computed metrics	RF	5-fold CV	AUC = 0.98(II/III), AUC = 1.00(II/IV), AUC = 0.97(III/IV), AUC = 0.88(IDH status)	Total = 381 (57II, 63III, 261IV)	Internal	De Looze et al.	2018	[85]
Purpose	Type	Modality	Feature	Classifier	Validation	Accuracy	Number of subjects	Data base[a]	Author	Year	References
Classification	Brain Tumour	T1WI, T2WI	3D texture attributes	SVM	LOOCV	AUC = 0.86	Total = 134 (45 MB, 71PA, 19EP)	Multi-center	Fetit et al.	2018	[86]
Classification	LGGs	cT1WI,T2WI, FLAIR	Radiomic features	SVM	5-fold CV	0.87	Total = 21 1p/19q intact, 26 1p/19q codeleted	Internal	Shofty et al.	2018	[87]

Table 4 (continued)

Purpose	Type	Modality	Feature	Classifier	Validation	Accuracy	Number of subjects	Data base[a]	Author	Year	References
Classification	Brain tumor	MRS	MRS feature	SVM	10-fold CV	0.86	Total = 41(17 medullo-blastomas, 20 pilocytic astrocytomas, 4 ependymo-mas)	Internal	Zarinabad et al.	2018	[88]
Stratification	Pseudo-/true progression	MRI, DTI	FA	SVM	10-fold CV	0.87	Total = 35 GB (13PsP, 22TTP)	Internal	Qian et al.	2016	[89]
Stratification	Pseudo-/true progression	MRI, DTI	FA	SVM	5-fold CV	AUC = 0.87	Total = 79 GBM (23PsP. 56TTP)	Internal	Zhang et al.	2016	[90]
Prediction	Glioma, 4 year survival asso-ciations	cT1WI, T2WI, FLAIR, DWI, DSC-MRI	Computed metrics	SVM	10-fold CV	AUC = 0.82	Total = 94 (31II, 14III, 49IV)	Internal	Emblem et al.	2014	[91]
Prediction	Glioma, 3 years survival asso-ciations	MRI, DWI, DSC-MRI	Computed metrics	SVM	Training/test (101/134)	AUC = 0.851	Training = 101, test = 134, total = 235	Internal	Emblem et al.	2015	[92]
Prediction	Glioblastoma, overall sur-vival	MT1WI, T2WI, FLAIR, DTI, DSC-MRI	Computed metrics	SVM	Training/test (34/31)	AUC = 0.84	Training = 34, test = 31, Total = 65	Internal	Akbari et al.	2016	[93]
Prediction	Glioblastoma, recurrence location	T1WI, FLAI	Volumetric, shape, tex-ture, paramet-ric, histogram features.	RF	Training/test (84/42)	AUC = 0.72	Training = 84, test = 42, total = 126	Internal	Chang et al.	2016	[94]
Prediction	Glioblastoma, methylation status	T1WI, T2WI	Co-occurrence, run length texture fea-tures	SVM	N/A	AUC = 0.85	Total = 155 (66 methylated, 89 unmethylated)	Internal	Korfiatis et al.	2016	[95]
Prediction	Glioblastoma, molecular subtypes	T1WI, cT1WI, T2WI, FLAIR, DTI, DSC-MRI	Imaging fea-tures	SVM	Training/test (105/29)	0.76	Train-ing = 105 GB, test = 29 GB, total = 134	Internal	Macyszyn et al.	2016	[96]
Prediction	LGG, Chro-mosomal Arms 1P/19q deletion	cT1WI,T2WI	Image intensity	CNN	Training/ test (387/90 slices)	0.88	Total = 159LGG (97OS, 45OD, 17AC)	Internal	Akkus et al.	2017	[97]

Table 4 (continued)

Purpose	Type	Modality	Feature	Classifier	Validation	Accuracy	Number of subjects	Data base[a]	Author	Year	References
Prediction	Glioma, MGMT/IDH1 status	rs-fMRI, DTI	Metrics, networks, regions, clinical feature	MIMC	10-fold CV	0.7174 (MGMT), 0.83(IDH1)	Total = 47 MGMT (26 positive, 20 negative, 1 unlabeled), 44 IDH1 (13 positive, 33 negative, 1 unlabeled)	Internal	Chen et al.	2017	[98]
Prediction	Glioma, IDH genotype of HGG	T1WI, T2WI, DWI	Imaging features	RF	Training/test (90/30)	0.89	Total = 120 (35III, 85IV)	N/A	Zhang et al.	2017	[99]
Prediction	GBM, survival group	cT1WI, T2WI, FLAIR	Signal intensity	SVM	LOOCV	0.88	Total = 32GBM	TCGA	Zhou et al.	2017	[100]
Prediction	LGG, p53 status	T2WI	Radiomic features	SVM	Training/test (180/92)	AUC = 0.763	Training = 180 gliomas (II/III), Test = 92 gliomas (II/III), total = 272	Internal	Li et al.	2018	[101]
Prediction	Glioma, survival	11C-MET PET	Image, ex vivo, patient features	Geometric probability covering algorithms	MCCV	0.89	Total = 70 (1I, 21II, 31III, 17IV)	Internal	Papp et al.	2018	[102]

N/A indicates information was not available or could not be found

[a]Internal: subjects were recruited from insitutional and/or public through media channels

Table 5 Summary of schizophrenia studies

Purpose	Disease	Modality	Feature	Classifier	Validation	Accuracy	Number of subjects	Data base[a]	Author	Year	References
Classification	SCZ/bipolar illness	sMRI, rs-fMRI	Functional connectivity (thalamas seeded)	SVM	LOOCV	0.74	SCZ = 90, HC = 90, total = 180	Internal	Anticevic et al.	2014	[103]
Classification	SCZ	T1WI, T2*WI, fMRI (working memory task)	MVPA, GLM	SBFE	LTOCV	0.91	P = 17 pure SCZ, 16 SCZ-OCD, HC = 20, total = 37	Internal	Bleich-Cohen et al.	2014	[104]
Classification	SCZ	T1WI	SBM	Bagged SVM	LOOCV	0.73	SCZ = 110, HC = 124, total = 234	Multisite	Castro et al.	2014	[105]
Classification	SCZ/BPD	T1WI	GM density	SVM	Training/test (198/136)	0.9(SCZ vs HC), 0.88(SCZ vs BPD), 0.67(BPD vs HC)	*P* = 66 SCZ, 66 BPD, HC = 66, total = 198	Internal	Schnack et al.	2014	[106]
Classification	SCZ	rs-fMRI	Functional network	SVM	LOOCV	0.79	SCZ = 19, HC = 29, total = 48	Internal	Cheng et al.	2015	[107]
Classification	SCZ, AH	T1WI, fMRI	Local fMRI activity measures	SVM	10-fold CV	1.00	*P* = 26 SCZ-AH (14 SCZ, 12 SAD, 1 SPD), 14 SCZ (5 SCZ, 8 SAD, 1 SPD), HC = 28, total = 68	Internal	Chyzhyk et al.	2015	[108]
Classification	SCZ	MPRAGE, rs-fMRI	Functional activity map features	Ensemble ELM, SLFN	10-fold CV	0.91	SCZ = 73, HC = 74, total = 147	Internal	Chyzhyk et al.	2015	[109]
Classification	SCZ	fMRI, MPRAGE	Regional fMRI activation pattern	SVM	LOOCV	0.93	SCZ = 44, HC = 44, total = 88	Internal	Koch et al.	2015	[110]
Classification	SCZ	T1WI	Voxel intensity	SVM	k-fold CV	0.92	SCZ = 19, HC = 16, total = 35	Internal	Chu et al.	2016	[111]
Classification	SCZ	rs-fMRI	Functional connectivity	DNN	5-fold CV	0.86	SCZ = 50, HC = 50, total = 100	NITRC	Kim et al.	2016	[112]
Classification	SCZ	T1WI	Voxel intensity	SVM		0.88	SCZ = 41, HC = 42, total = 83	Internal	Lu et al.	2016	[113]
Classification	SCZ	T1WI	Cortical thickness, anatomical structure volume	DBN	3-fold CV	0.74	SCZ = 143, HC = 83, total = 226	Internal	Pinaya et al.	2016	[114]

Table 5 (continued)

Purpose	Disease	Modality	Feature	Classifier	Validation	Accuracy	Number of subjects	Data base[a]	Author	Year	References
Classification	SCZ/SIB	MRI	Thalamic grey matter volume	RF	LOOCV	0.81(SCZ vs HC), 0.75(SIB vs HC)	SCZ = 96, SIB = 55, HC = 249, total = 400	Internal	Pergola et al.	2017	[115]
Classification	SCZ/PD	rs-fMRI	Functional conncetivity (thalamas seeded)	SVM	10-fold CV	0.72	SCZ = 86, HC = 84HC, total = 170	COBRE	Pläschke et al.	2017	[116]
Classification	SCZ	MPRAGE, rs-fMRI	Cortex structural features, global connectivity measure	ELM	10-fold CV	1.00	SCZ = 72, HC = 72, total = 144	COBRE	Qureshi et al.	2017	[117]
Classification	SSD	fMRI	Functional conncetivity (thalamas seeded)	Regularized linear discriminant analysis classifiers	Training/test (373/147)	0.77	SCZ = 182 HC = 348, total = 530	Multisite	Skåtun et al.	2017	[118]
Classification	SCZ	T1WI	Segmented GM, WM, CSF, behavioural analysis	SVM	LOOCV	0.94	SCZ = 17, HR = 17, total = 34	N/A	Zarogianni et al.	2017	[119]
Classification	SCZ	rs-fMRI	3D spatial maps	SVM	LOOCV	0.98	SCZ = 25, HC = 25, total = 50	BIRN	Juneja et al.	2018	[120]
Classification	SSD	DTI	FA	SVM	LTOCV	0.62	SCZ = 77, HC = 77, total = 154	Internal	Mikolas et al.	2018	[121]
Classification	SCZ	fMRI	Functional connectomes	SVM	LSOCV	0.84	SCZ = 191HC = 191, total = 382	Multisite	Orban et al.	2018	[122]
Classification	SCZ	fMRI	Functional connectivity	Deep DANS NN	LSOCV	0.85	SCZ = 474HC = 607, total = 1081	Multisite	Zeng et al.	2018	[123]

N/A indicates information was not available or could not be found

[a]Internal: subjects were recruited from insitutional and/or public through media channels

Table 6 Summary of depressive disorder studies

Purpose	Type	Modality	Feature	Classifier	Validation	Overall accuracy	Number of subjects	Data base[a]	Author	Year	References
Classification	MDD	rs-fMRI	Functional connectivity	SVM	LOOCV	0.84	MDD = 39, HC = 37, total = 76	Internal	Cao et al.	2014	[125]
Classification	DEP	DTI	FA map	SVM	LOOCV	0.83	DEP = 29, HC = 30, total = 59	Internal	Qin et al.	2014	[126]
Classification	MDD	rs-fMRI	Connectivity patterns	LG-MMC	LOOCV	0.93	MDD = 24, HC = 29, total = 53	Internal	Zeng et al.	2014	[127]
Classification	depressive comorbidity, panic disorder	fMRI	Beta values, *t*-statistic images	SVM	LOOCV	0.79	PD (−DEP) = 33, PD (+DEP) = 26	Internal	Lueken et al.	2015	[128]
Classification	cMDD, rMDD	DTI, fMRI	5 physiological parameters, 3 network measures	SVM	LOOCV	1.00(DEP vs HC), 0.9767(cMDD vs rMDD)	cMDD = 28, rMDD = 15, HC = 30, total = 73	Internal	Qin et al.	2015	[129]
Classification	MDD	fMRI	PPI t-maps	MLDA	LOSOCV	0.78	MDD = 25, HC = 21, total = 46	Internal	Sato et al.	2015	[130]
Classification	DEP	fMRI (verbal fluency)	Brain activity *Z* scores	SVM	10-fold CV	0.95	DEP = 31, HC = 31, total = 62	Internal	Shimizu et al.	2015	[131]
Classification	PUD	T1WI	Morphometric measurements	SVM	LOOCV	0.78	PUD = 25, 2HC = 6, total = 31	Internal	Wu et al.	2015	[132]
Classification	MDD, severity	rs-fMRI, fMRI (emotional-face)	fMRI volume space (masked)	SVM	5-fold CV	0.66(severe), 0.58(mild to moderate)	MDD = 45, HC = 19, total = 64	Internal	Ramasubbu et al.	2016	[133]
Classification	MDD	rs-fMRI	Connectivity patterns	SVM + elastic net	LOOCV	0.76	MDD = 38, HC = 29, total = 67	Multi site	Bhaumik et al.	2017	[134]
Classification	MDD	[carbonyl-11C] WAY-100635 PET, 3D T1WI	PET data	SVM	10-fold CV	0.75	MDD = 19, HC = 62, total = 81	Internal	Kautzky et al.	2017	[135]
Classification	MDD	DTI	FA map	SVM	LOSPGOCV	0.76	MDD = 25, HC = 25, total = 50	Internal	Schnyer et al.	2017	[136]
Classification	MDD, ECT	3D T1WI, rs-fMRI	GM volume, functional connectivity	SVM	LOOCV	0.83	MDD = 23, HC = 25, total = 48	Internal	Wang et al.	2017	[137]

Table 6 (continued)

Purpose	Type	Modality	Feature	Classifier	Validation	Overall accuracy	Number of subjects	Data base[a]	Author	Year	References
Classification	MDD, BD	DTI	Tract profiles	SVM	N/A	0.68	BD = 31, MDD = 36, HC = 45, total = 112	Internal	Deng et al.	2018	[138]
Classification	MDD	[Carbonyl-11C] WAY-100635 PET, T1WI	PET data	MVPA	LOOCV	AUC = 0.58(MDD vs HC), AUC = 0.80(HR vs HC), AUC = 0.49(MDD vs HR)	N/A	N/A	Milak et al.	2018	[139]
Prediction	MDD, first onset	T1WI	Cortical thickness	SVM	10-fold CV	0.70	MDD = 18, HC = 15, total = 33	Internal	Foland-Ross et al.	2015	[140]
Prediction	TRD	MPRAGE	GM volume	SVM	LOOCV	0.85	TRD = 20, HC = 21, total = 41	Internal	Johnston et al.	2015	[141]
Prediction	Late-life depression, treatment response	T1WI, T2WI, DTI, rs-fMRI	functional, Structural image features	SVM	LOOCV	0.8727 (late-life), 0.8947 (treat. response)	DEP = 22 (late-life), 19 (treat. response), HC = 28, total = 69	Internal	Patel et al.	2015	[142]
Prediction	ECT response	sMRI	Voxel-based morphometry	SVM	LOSOCV	0.78	ECT = 23, medication = 23, HC = 21, total = 67	Internal	Redlich et al.	2016	[143]
Prediction	Clinical depression scores	rs-fMRI	Functional connectivity	KPLS-poly + LDA	LOOCV	0.81	DEP = 58, HC = 65, total = 123	Internal	Yoshida et al.	2017	[144]

N/A indicates information was not available or could not be found

[a]Internal: subjects were recruited from insitutional and/or public through media channels

Table 7 Summary of Parkinson's disease studies

Purpose	Type	Modality	Features	Classifier	Validation	Overall accuracy	Number of Subjects	Data base[a]	Author	Year	References
Classification	PD	T1WI	WM, GM, CSF volume in 98 ROIs	LS-SVM	10-fold CV	0.82	PD = 374, NC = 169, total = 543	PPMI	Adeli et al.	2016	[145]
Classification	PD, non-PD	FP-CIT SPECT	Uptake measures	Elastic-Net	Training/test (379/75)	0.99	PD = 72, SWEDD = 77, HC = 10, total = 159	PPMI + internal	Choi et al.	2017	[146]
Classification	PD	T1WI	Multilevel ROI features	JFSS + LDA	10-fold CV	0.86	PD = 69, HC = 103, total = 172	PPMI	Peng et al.	2017	[147]
Classification	PD	T1WI	Network measures, clinical scores	RF + SVM	10-fold CV	0.93	PD = 374, NC = 169, total = 543	PPMI	Amoroso et al.	2018	[148]
Classification	PD	FP-CIT SPECT	CSF, RNA, Serum test, image features	SVM	LOOCV	0.97	PD = 168, SWEDD = 26, HC = 194, total = 388	PPMI	Castillo-Barnes et al.	2018	[149]
Classification	PD	FP-CIT SPECT	Uptake measures	deep CNN	LOOCV	0.98	PD = 443, HC = 209, Total = 652	PPMI	Oliveira et al.	2018	[150]
Differentiation	PD, PSP	3D T1WI	Voxel-based pattern distribution	EPNN	LOOCV	0.858 (PD vs HC), 0.89(PSP vs HC), 0.89 (PD vs PSP)	PD = 28, PSP = 28, HC = 28, total = 84	Internal	Salvatore et al.	2014	[151]
Differentiation	PD, SWEDD	FP-CIT SPECT	Motor, non-motor, neuroimaging features	EPNN	10-fold CV	0.925(PD vs HC), AUC = 0.97 (SWEDD vs HC), 0.97(PD vs SWEDD)	N/A	PPMI	Hirschauer et al.	2015	[152]
Differentiation	PD, vascular PD	FP-CIT SPECT	Uptake measures	RLDA	10-fold CV	0.90	VPD = 80, PD = 164, total = 244	Internal	Huertas-Fernández et al.	2015	[153]
Differentiation	PD, SWEDD	T1WI	WM, GM, KSOM feature	LS-SVM	8-fold CV	0.99	PD = 518, SWEDD = 68, HC = 245, total = 831	PPMI	Singh et al.	2015	[154]
Differentiation	PD	T1WI	WM, GM features	SVM	8-fold CV	0.71	PD = 56, HC = 56, total = 112	PPMI	Liu et al.	2016	[155]

Table 7 (continued)

Purpose	Type	Modality	Features	Classifier	Validation	Overall accuracy	Number of Subjects	Data base[a]	Author	Year	References
Differentiation	PD, MSA, PSP	DTI, R2*WI	FA, MD	SVM	10-fold CV	AUC = 0.88 (HC vs PD/MSA/PSP), 0.91 (HC vs PD), 0.94(PD vs MSA/PSP), 0.99(PD vs MSA), 0.99(PD vs PSP), 0.98(MSA vs PSP)	PD = 35, MSA = 16, PSP = 19, HC = 36, total = 106	Internal	Du et al.	2017	[156]
Prediction	PD, treatment response	DWI, fMRI	Subject-level general linear model	SVM	LOOCV	0.85	PD = 34, HC = 42, total = 76	Internal	Ye et al.	2016	[157]

N/A indicates information was not available or could not be found

[a]Internal: subjects were recruited from institutional and/or public through media channels

Parkinson's disease

The main purposes of ML studies on PD were classification and differentiation of PD from normal control (NC), progressive supranuclear palsy (PSP), and/or subjects with scans without evidence of dopaminergic deficit (SWEDD). We surveyed 13 papers, which are presented in Table 7.

Attention-deficit hyperactivity disorder

ADHD is one of the most commonly found functional disorders affecting children. In 2011, a global competition (called ADHD-200) was held to use neuroimaging as well as phenotypic measures to automatically detect ADHD [158]. Approximately, half of the studies reviewed in this survey were based on that challenge. The main characteristics of those studies are tabulated in Table 8.

Autism

ASD is a common disorder affecting youth, and share a high degree of comorbidity with other psychiatric disorders [170]. Both autism spectrum disorder (ASD) and ADHD are currently diagnosed on the basis of parent interview and clinical observation [171]. The identification of objective and reliable biomarkers is thus a critical yet elusive goal for neuroimaging researchers [172]. We surveyed 11 papers in classification of ASD mostly using functional MRI-based features and a prediction of ASD severity based on structure MRI. Those studies are listed in Table 9.

Epilepsy

The main purposes of ML studies on epilepsy were classification of epilepsy from other type of diseases, detection, and prediction of treatment outcome. MR imaging was a main modality used for ML studies. Depending on the purpose, variety of MR imaging methods, such as T1WI and DTI were employed. Table 10 summarizes the epilepsy studies.

Multiple sclerosis

The main purposes of ML studies on MS were classification, detection, and segmentation of MS lesion. Both structural and functional MRI were the main imaging methods used for ML studies. Table 11 summarizes the MS studies.

Stroke

ML techniques have been applied for stroke imaging in two different aspects: i.e., automatic or accurate diagnosis and

Table 8 Summary of ADHD studies

Purpose	Type	Modality	Feature	Classifier	Validation	Overall accuracy	Number of subjects	Data base[a]	Author	Year	References
Classification	ADHD, TDC, ADHD-I, ADHD-C	T1WI	Cortical features	SVM, ELM	10-fold CV	0.61	935	ADHD-200 dataset	Qureshi et al.	2016	[159]
Classification	ADHD, TDC, ADHD-I, ADHD-C	MRI, rs-fMRI	Structural, functional	SVM, ELM	Training/test (159/42)	0.76	935	ADHD-200 dataset	Qureshi et al.	2017	[160]
Classification	ADHD	T1WI, fMRI	Functional	SVM	10-fold CV	0.69	215	ADHD-200 dataset	Tan et al.	2017	[161]
Identification	ADHD	fMRI	Individual statistical maps	SVM (Gaussian process classifier)	LOOCV	0.77	60	Internal	Hart et al.	2014	[162]
Identification	ADHD	T1WI	T1WI	SVM	LOOCV	0.93	68	Internal	Johnston et al.	2014	[163]
Identification	ADHD	MRI, fMRI	HOG	SVM	5-fold CV	0.70	940	ADHD-200 dataset	Ghiassian et al.	2016	[164]
Identification	ADHD	MRI, fMRI	HOG	SVM	5-fold CV	0.65	1111	ABIDE	Ghiassian et al.	2016	[164]
Identification	ADHD	MRI	Structural	Least absolute shrinkage and selection operator (Lasso)	LOOCV	0.81	47	Internal	Xiao et al.	2016	[165]
Identification	ADHD	T1WI, DTI	GM, WM volume, FA, TR	SVM (non-linear GRBF kernel)	10-fold CV	0.66	133	Internal	Chaim-Avancini et al.	2017	[166]
Identification	ADHD	fMRI	Imaging + non-imaging data	SVM	LOOCV	0.87	N/A	ADHD-200 dataset	Riaz et al.	2018	[167]
Identification	ADHD	MRI, fMRI	Structural, functional	SVM	5-fold CV	0.67	729	ADHD-200 dataset	Sen et al.	2018	[168]
Identification	ADHD	fMRI	Structural, functional	SVM	5-fold CV	0.64	1099	ABIDE	Sen et al.	2018	[168]
Prediction	ADHD, treatment responder	fMRI	N/A	SVM (second-order polynomial kernel)	10-fold CV	0.85	N/A	Internal	Kim et al.	2015	[169]

N/A indicates information was not available or could not be found

[a]Internal: subjects were recruited from insitutional and/or public through media channels

Table 9 Summary of autism studies

Purpose	Disease	Modality	Features	Classifier	Validation	Overall accuracy	Number of subjects	Data base[a]	Author	Year	References
Classification	Autism	fMRI, HRADI	Group level factors	GNB	N/A	0.97	Autism = 17, NC = 17, total = 34	Internal	Just et al.	2014	[173]
Classification	ASD	rs-fMR	Connectivity	RF	out-of-bag	0.91	ASD = 126, TD = 126TD, Total = 252	ABIDE	Chen et al.	2015	[174]
Classification	ASD	T1WI	Morphological	SVM	LPOCV	AUC = 0.74	ASD = 21, NC = 20, total = 41	Internal	Gori et al.	2015	[175]
Classification	ASD	rs-fMRI	Connectivity	PNN	LOOCV	0.90	ASD = 312, TD = 328TD, total = 640	ABIDE	Iidaka et al.	2015	[176]
Classification	ASD	rs-fMRI	Connectivity	L2LR	LOOCV	0.77	ASD = 59, TD = 59TD, total = 118	ABIDE	Plitt et al.	2015	[177]
classification	ASD	rs-fMRI	Connectivity	RF	out-of-bag	0.71	ASD = 126, NC = 126, Total = 252	ABIDE	Jahedi et al.	2017	[178]
Classification	ASD	rs-fMRI	Connectivity	DRBMs	10-fold CV	0.81	ASD = 61, NC = 72, total = 133	ABIDE(UM)	Kam et al.	2017	[179]
Classification	ASD	rs-fMRI, sMRI	Connectivity, structure	DBN	10-fold CV	0.66	ASD = 116, NC = 69, total = 185	ABIDE I, II	Aghdam et al.	2018	[180]
Classification	ASD	rs-fMRI	Connectivity	random SVM cluster	Training/test (58/26)	0.96	ASD = 45, TD = 39TD, Total = 84	ABIDE	Bi et al.	2018	[181]
Classification	ASD	rs-fMRI	Functional activity	DNN	10-fold CV	0.70	ASD = 505, NC = 530, total = 1035	ABIDE	Heinsfeld et al.	2018	[182]
Classification	ASD	rs-fMRI	Connectivity	DTL-NN	5-fold CV	0.67	ASD = 149, NC = 161, total = 310	ABIDE	Li et al.	2018	[183]
Prediction	ASD, severity	T1WI	Cortical thickness	SVM	10-fold CV	$r = 0.51 \pm 0.04$	ASD = 156	ABIDE	Moradi et al.	2017	[184]

N/A indicates information was not available or could not be found

[a]Internal: subjects were recruited from insitutional and/or public through media channels

Table 10 Summary of epilepsy studies

Purpose	Tyep	Modality	Feature	Classifier	Validation	Overall accuracy	Number of subjects	Data base[a]	Author	Year	References
Classification	Epilepsy, MTS	MPRAGE	Morphological measures	SVM-RFE	10-fold CV	0.81	wMTS = 85, w/oMTS = 84	Internal	Rudie et al.	2015	[185]
Classification	Epilepsy, FCD	T2WI	Cortical thickness	SVM	LOOCV	0.98	FCD type I = 13, type II = 28, NC = 41, total = 82	Internal	Hong et al.	2016	[186]
Classification	TLE, lateralization	DTI	Structural connectomes	SVM	LOOCV	0.897 (right), 0.86 (left), 0.864 (control)	TLE = 44, NC = 14, total = 58	Internal	Kamiya et al.	2016	[187]
Classification	TLE	DTI, DKI	Diffusion metrics	SVM	5-fold CV	0.82	Epilepsy = 32, NC = 36, total = 68	Internal	Del Gaizo et al.	2017	[188]
Detection	Epilepsy, cortial dysplasia type II	MRI	Surface-based features	LDA	LOOCV	0.74 (sensitivity)	Epilepsy = 19, NC = 24, total = 43	Internal	Hong et al.	2014	[189]
Detection	Epilepsy	T1WI	Texture parameters	OC-SVM	N/A	0.769 (sensitivity)	Epilepsy = 11 NC = 77, total = 88	Internal	Azami et a.l	2016	[190]
Detection	Epilepsy	T1WI	Surface-based features	NN	LOOCV	0.87 (AUC)	Epilepsy = 22, NC = 28, Total = 50	Internal	Adler et al.	2017	[191]
Prediction	TLE, treatment outcome	T1WI	Surface-based features	*k*-Means clustering	LOOCV	0.81	TLE-I = 24, TLE-II = 32, TLE-III = 34, TLE-IV = 24, NC = 42, total = 156	Internal	Bernhardt et al.	2015	[192]
Prediction	Epilepsy, treatment outcome	DTI	Structural connectome	Elastic net	10-fold CV	0.80	Epilepsy = 35, NC = 18, total = 53	Internal	Munsell et al.	2015	[193]
Prediction	Epilepsy, laterality	PET, MRI, and DTI	Glucose metabolism, cortical thickness, WM atrophy	Logistic regression	N/A	1.00	Left TLE = 28, right TLE = 30	Internal	Pustina et al.	2015	[194]

N/A indicates information was not available or could not be found

[a]Internal: subjects were recruited from insitutional and/or public through media channels

Table 11 Summary of multiple sclerosis studies

Purpose	Type	Modality	Feature	Classifier	Validation	Overall accuracy	Number of subjects	Data base[a]	Author	Year	References
Classification	Motor function	rs-fMRI, DTI	GMM + FC	SVM	LOOCV	0.8834 (HC vs MI), 0.84 (HC vs MP), 0.86 (MP vs MI)	MP = 26MP, MI = 25, NC = 21, total = 72	Internal	Zhong et al.	2017	[195]
Classification	MS, NAWM, HC	MRI	Myelin, T1WI features	Deep CNN, RF	11-fold CV	0.88	MS = 55, NC = 44, total = 99	Internal	Yoo et al.	2018	[196]
Classification	Relapsing-remitting MS	T1WI, rs-fMRI, DTI	FA, connectivity, function correlation	SVM	10-fold CV, LOOCV	0.89	MS = 104, NC = 46, total = 150	Internal	Zurita et al.	2018	[197]
Detection	MS new lesion	rs-fMRI	Functional connectivity	SVM, RF	5-fold CV	0.86	MS = 18, NC = 19, total = 37	Internal	Saccà et al.	2018	[198]
Detection	MS	T2WI	DF information	LRM	LOOCV	0.77	MS = 36	Internal	Salem et al.	2018	[199]
Prediction	Worsening cases	T2WI	Normalized T2 hyperintense lesion volume (T2LV)	SVM + bagging	10-fold CV	0.62	MS = 1693	CLIMB	Zhao et al.	2017	[200]
Segmentation	MS lesion	T1WI, MPRAGE, T2WI, PDWI, FLAIR	structural	Dictionary learning	LOSOCV	0.50	MS = 14	Internal	Deshpande et al.	2015	[201]
Segmentation	MS lesion	MPRAGE, MP2RAGE, FLAIR, DIR	Image intensity	k-NN	LOOCV	0.75	MS = 39	Internal	Fartaria et al.	2016	[202]

[a]Internal: subjects were recruited from insitutional and/or public through media channels

prediction of prognosis [203]. Automatic lesion identification or segmentation is one of the most important elements in precision medicine dealing with huge datasets of brain imaging. This is because manual lesion segmentation is cumbersome and inconsistent across raters [204]. Prediction of treatment complications may be useful for screening a high-risk group receiving acute treatment, such as thrombolysis [205], whereas prediction of neurological long-term outcomes may guide the stroke management [206]. Both CT and structural MRI were a main modalities. Table 12 summarizes the stroke studies.

Traumatic brain injury

Neuroimaging plays a critical role in the acute setting to guide appropriate management by detecting injuries that require intervention or further monitoring [214]. Among various MR imaging techniques, the DTI metrics are thought to reflect the integrity of microstructural properties of white matter and have been applied extensively as neuroimaging biomarkers to study a range of clinical conditions [215]. The main purposes of ML studies on TBI were classification of mild traumatic brain injury (mTBI) from NC and/or post concussion syndrome (PCS) and posttraumatic stress disorder (PTSD). CT, DTI, and fMRI were the main modality used for ML studies on TBI. Table 13 summarizes the TBI studies.

Study characteristics

Number of publications

Figure 2 shows the number of papers published in each year for each disease type. The number of studies showed a growing trend since 2014 (2018 was not an entire year, the term was 1 January–19 September). As shown in Table 2, top three researches are strongly supported by big data sets. Typically, 92.7% of AD/MCI studies were carried out on large data sets, such as ADNI, OASIS [223], DZNE [224], PRODEM [225], and AIBL [226]. This clearly indicates that the well-maintained database supports the progress of technology and their publications.

Overall accuracy vs. total sample size

Figure 3 shows the overall accuracy against the total sample size used in the studies. Almost all studies that reported very high accuracies (69.8% of studies were higher than 0.8) had sample sizes smaller than 100 (45.6% of studies). The reported overall accuracy decreases with sample size in most of the disorders, such as schizophrenia and ADHD. This pattern raises a serious concern regarding generalizability of many of those studies with small sample sizes. On the other hands, only PD studies (* in Fig. 3) showed positive relationships between the accuracy and the total sample size. Parkinson's Progression Markers Initiative (PPMI) may play an important role. In contrast, the result of MRI measures varies from facility-to-facility and the standardization still appears to be an open problem [227].

Total sample size distribution

Figure 4 shows the sample size distribution. The dashed lines represent mean (red) and median (blue) sizes, which are 231 and 120, respectively.

When using diagnosis models that are very complex or have many parameters on datasets with small number of samples, overfitting tends to take place. Usually, ML creates classifier from training dataset. In the training session, ML sometimes extracts unique characteristics, which are only based on the training datasets. Therefore, an overfitted model provides good results on the training data and poor results on the test data. Neuroimaging datasets tend to have limited sample size and millions of voxels per sample. The majority of surveyed studies built predictive models based on a very small number of subjects. Therefore, it is plausible that many surveyed studies suffer from overfitting problem. Cross validation, simple classifier, and proper feature selections can help avoid overfitting.

Accuracy for each disorder

Figure 5 illustrates the summary statistics of reported overall accuracy for each disorder. AD/MCI and PD studies exceeded 0.9 in median. In contrast, ADHD and stroke studies were less than 0.7 in their medians. Others had around 0.8 to < 0.9 in their median of accuracy.

Classification method

Figure 6 shows the classifiers used in the studies. In terms of classification methods, support vector machine (SVM) was still the most popular method (more than 55%, 117/209 papers). Different strategy of SVM such as linear, non-linear with different kernel, SVM with recursive feature elimination, SVM with L1 regularization and SVM with L1 and L2 regularization (elastic net) have been used for classification of various disorders.

Although deep neural network (DNN) is attracting attention in recent years [203, 228, 229], there were still only 18 papers published in the last 5 years using DNN. Additionally, random forest (RF) was used in 11 papers.

Table 12 Summary of stroke studies

Purpose	Type	Modality	Feature	Classifier	Validation	Overall accuracy	Number of subjects	Data base[a]	Author	Year	References
Detection	Early infarction signs	CT	ASPECTS score	e-ASPECTS, version 6.0[b]	N/A	0.67	Stroke = 119	Internal	Guberina et al.	2018	[207]
Identification	Motor disability	rs-fMRI	Resting-state connectivity	SVM	LOOCV	0.88	Stroke = 20 (Training), 20 (test), NC = 20, Total = 60	Internal	Rehme et al.	2015	[208]
Prediction	Post intra-arterial therapy outcome	CT	The presence of acute stroke and intracranial haemorrhage	ANN, SVM	LOOCV	0.87	Stroke = 107	Internal	Asadi et al.	2014	[209]
Prediction	Thrombolysis outcome, SICH	CT	CT-value	SVM	10-fold CV	0.744 (AUC)	SICH = 63, noSICH = 49	Internal	Bentley et al.	2014	[210]
Segmentation	Stroke lesion	MRI	Intensity feature, the weighted local mean, the 2D center distance and the local histogram	RDF	N/A	0.67	Stroke = 37	Internal	Maier et al.	2015	[211]
Segmentation	Chronic stroke lesion	T1WI	Feature map	Gaussian naïve Bayes	LOOCV	0.66	Stroke = 30	Internal	Griffis et al.	2016	[212]
Segmentation	Chronic stroke lesion	T1WI	12 geometric features	LINDA	6-fold CV	0.696	Stroke = 60 (training), 45 (test), NC = 80, total = 185	Internal	Pustina et al.	2016	[213]

N/A indicates information was not available or could not be found

[a]Internal: subjects were recruited from insitutional and/or public through media channels

[b]e-ASPECTS. Brainomix®, Oxford, UK. https://www.brainomix.com/ (accessed 10/2018)

Table 13 Summary of traumatic brain injury studies

Purpose	Type	Modality	Feature	Classifier	Validation	Overall accuracy	Number of patients	Data base[a]	Author	Year	References
Classification	TBI	DTI	FA measures, network connectivity	Decision ensemble	10-fold CV	0.68	TBI = 179, NC = 146, total = 325	Internal	Mitra et al.	2016	[216]
Classification	mTBI	CT	N/A	RF	10-fold CV	0.78	mTBI = 334 (179 training, 155 test), HC = 328, total = 662	Internal	Peacock IV et al.	2017	[217]
Classification	PTSD, mTBI	MRI, DTI	Static and dynamic functional connectivity	RF	6-fold CV	0.84	PTSD = 17, PCS + PTSD = 42, NC = 28, total = 87	Internal	Rangaprakash et al.	2017	[218]
Classification	mTBI	rs-fMRI, DTI	Network connectivity, FA	SVM	LOOCV	0.84	mTBI = 50, NC = 50, total = 100	Internal	Vergara et al.	2017	[219]
Classification	Disease foci	rs-fMRI	Effective connectivity networks	RF	6-fold CV	0.81	PTSD = 87, PCS + PTSD = 87, NC = 87, total = 261	Internal	Rangaprakash et al.	2018	[220]
Identification	TBI	DTI	WM connectivity	SVM	10-fold CV	0.93	TBI = 52, NC = 25, total = 77	Internal	Fagerholm et al.	2015	[221]
Prediction	Severity	CT	N/A	RCE-SVM	N/A	0.98 (AUC)	TBI = 39, NC = 156, total = 195	Internal	Chong et al.	2015	[222]

N/A indicates information was not available or could not be found

[a]Internal: subjects were recruited from insitutional and/or public through media channels

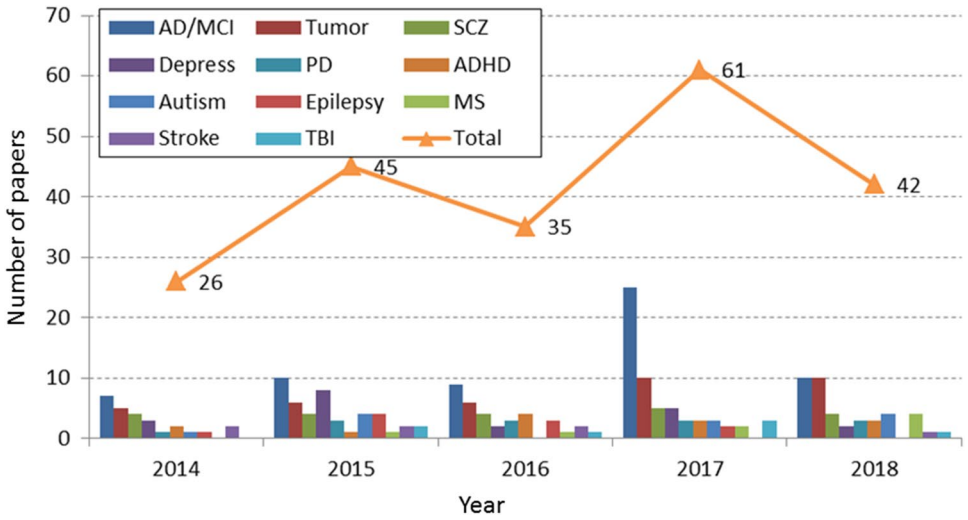

Fig. 2 Total number of papers within each year for every disease or disorder

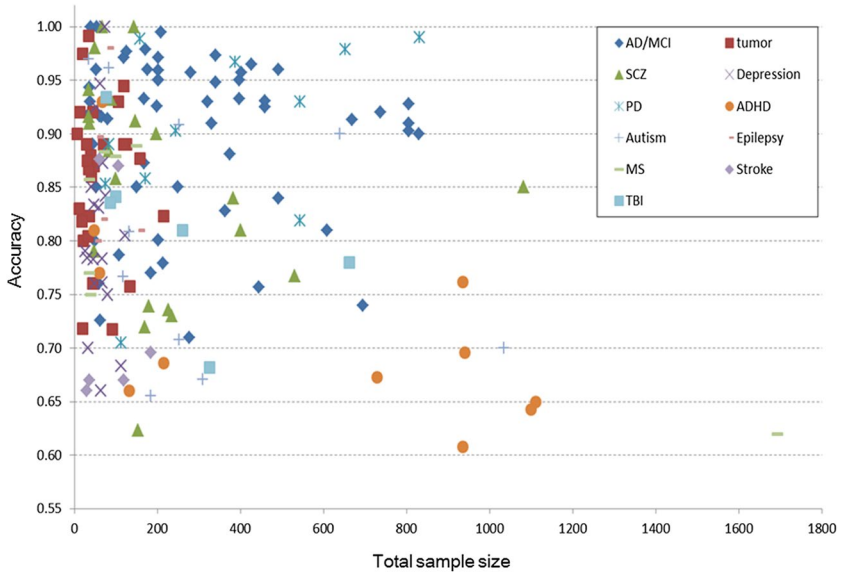

Fig. 3 Scatter plot of overall reported accuracy versus the total sample size

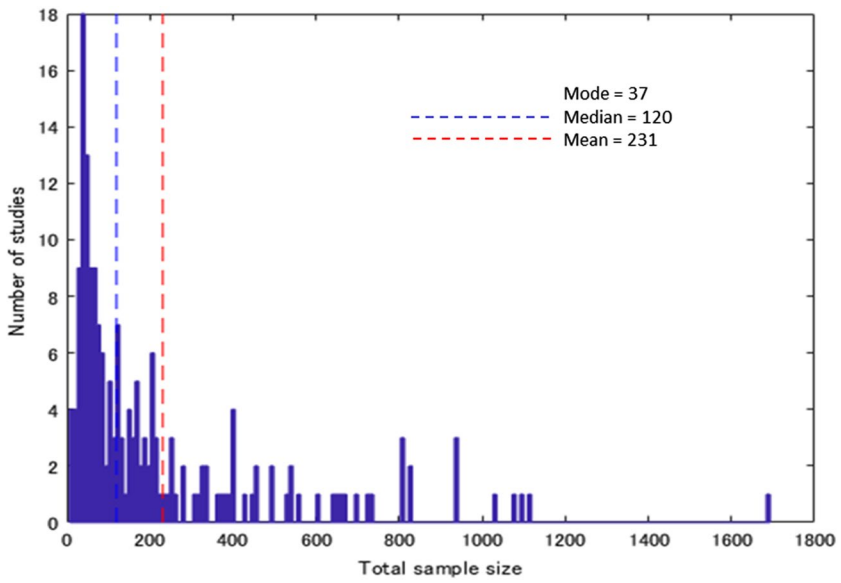

Fig. 4 Histogram of the sample sizes of the surveyed studies. Vertical dashed lines indicate mean (red) and median (blue) sample size among all studies, which are 231 and 120, respectively

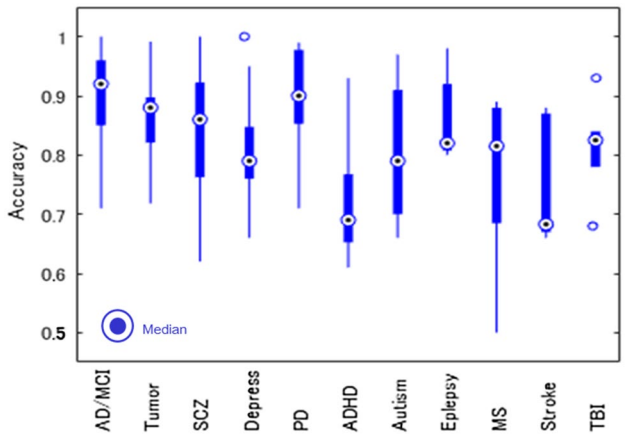

Fig. 5 Disorder-specific box plots of reported overall accuracies of the surveyed papers. Dot including circles indicate the median accuracy

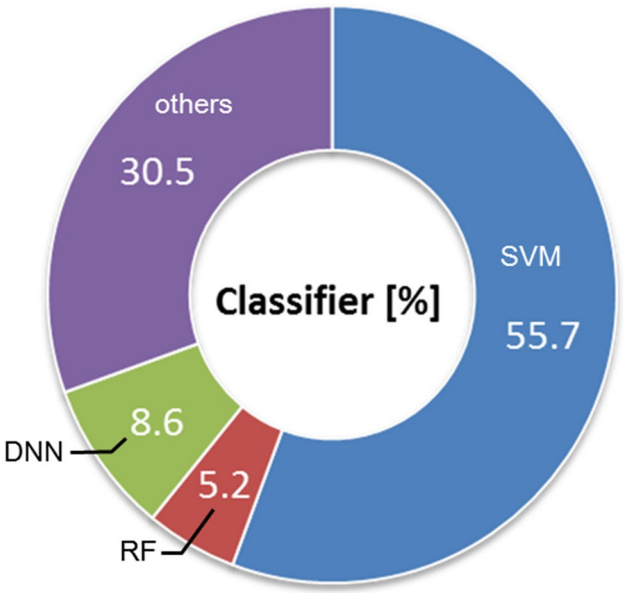

Fig. 6 Classifiers used for ML of the surveyed papers

Validation method

Figure 7 shows the validation methods used in the studies. In terms of classifier validation methods, *k*-hold cross validation (CV) is the most popular method (more than 80%, 169/209 papers). The constant k was varying; $k = 1–10$. Among them, the popular methods were leave-one-out cross validation (LOOCV) and tenfold CV.

Ideally, training/test scheme should be chosen for the validation of classifier, but more than 80% of papers made *k*-hold CV because of lack of subject. Only 9.1% (19 papers) made training/test scheme for the validation of classifier.

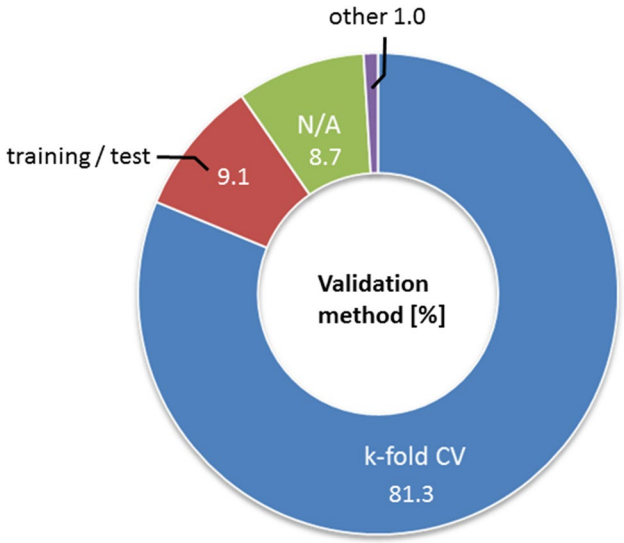

Fig. 7 Validation methods used for ML of the surveyed papers

Limitations

There are several limitations in this work. Firstly, we limited our search to English journal papers. Secondly, there are other studies based on other modalities such as EEG MEG, and US, which were not included in this study. Moreover, other important conditions such bipolar and anxiety disorders were not reviewed in this work. Many of the papers contained multiple experiments under different scenarios, such as multiple ML methods, data reduction methods, and multiple data sets, but we just reported one of the most successful remarks.

Summary

In this paper, we comprehensively reviewed 11 diseases neuroimaging-based 209 ML studies in the recent 5 years period of time. To clarify the recent trends of ML studies in the field of neuroradiology, we summarized ML methods used in these research, the number of data, image features, and the overall accuracy. We have also shown that there are several bottlenecks, such as feature selection bias and overfitting by small sample size.

It is clear that the result of ML, which is a statistical model fitting method, depends on its sample size. Therefore, as many previous review papers have pointed out, the existence of large data sets is indispensable for promoting ML study. More importantly, multidisciplinary cooperation remains a crucial aspect, and if achieved, Wang and Summers's expectations might become true.

Funding One of the authors (K. Y.) was funded by following companies (within the past 12 months): Nihon Medi-Physics Co., Ltd., Daiichi Sankyo Co., Ltd., Fuji Pharma Co.,Ltd., Doctor-Net Inc, and Fujifilm RI Pharma Co., Ltd.

Compliance with ethical standards

Ethical statements This article does not contain any studies with human participants or animals performed by any of the authors.

Conflict of interest The authors declare that they have no conflict of interest.

References

1. Wang S, Summers RM. Machine learning and radiology. Med Image Anal. 2012;16:933–51.
2. Arbabshirani MR, Plis S, Sui J, Calhoun VD. Single subject prediction of brain disorders in neuroimaging: promises and pitfalls. Neuroimage. 2017;145:137–65.
3. US national library of medicine national institutes of health. https://www.ncbi.nlm.nih.gov/pubmed/. Accessed Oct 2018.
4. Moher D. Preferred reporting items for systematic reviews and meta-analyses. J Clin Epidemiol. 2009;62:1006–12.
5. Jie B, Zhang D, Gao W, Wang Q, Wee CY, Shen D. Integration of network topological and connectivity properties for neuroimaging classification. IEEE Trans Biomed Eng. 2014;61(2):576–89.
6. Li M, Oishi K, He X, Qin Y, Gao F, Mori S, et al. An efficient approach for differentiating Alzheimer's disease from normal elderly based on multicenter MRI using gray-level invariant features. PLoS One. 2014;9(8):e105563.
7. Li M, Qin Y, Gao F, Zhu W, He X. Discriminative analysis of multivariate features from structural MRI and diffusion tensor images. Magn Reson Imaging. 2014;32(8):1043–51.
8. Li S, Yuan X, Pu F, Li D, Fan Y, Wu L, et al. Abnormal changes of multidimensional surface features using multivariate pattern classification in amnestic mild cognitive impairment patients. J Neurosci. 2014;34(32):10541–53.
9. Liu M, Zhang D, Shen D, Alzheimer's Disease Neuroimaging I. Identifying informative imaging biomarkers via tree structured sparse learning for AD diagnosis. Neuroinformatics. 2014;12(3):381–94.
10. Segovia F, Bastin C, Salmon E, Gorriz JM, Ramirez J, Phillips C. Combining PET images and neuropsychological test data for automatic diagnosis of Alzheimer's disease. PLoS One. 2014;9(2):e88687.
11. Suk HI, Lee SW, Shen D, Alzheimer's Disease Neuroimaging I. Hierarchical feature representation and multimodal fusion with deep learning for AD/MCI diagnosis. Neuroimage. 2014;101:569–82.
12. Cheng B, Liu M, Suk HI, Shen D, Zhang D, Alzheimer's Disease Neuroimaging I. Multimodal manifold-regularized transfer learning for MCI conversion prediction. Brain Imaging Behav. 2015;9(4):913–26.
13. Dyrba M, Grothe M, Kirste T, Teipel SJ. Multimodal analysis of functional and structural disconnection in Alzheimer's disease using multiple kernel SVM. Hum Brain Mapp. 2015;36(6):2118–31.
14. Farzan A, Mashohor S, Ramli AR, Mahmud R. Boosting diagnosis accuracy of Alzheimer's disease using high dimensional recognition of longitudinal brain atrophy patterns. Behav Brain Res. 2015;290:124–30.
15. Jie B, Zhang D, Cheng B, Shen D, Alzheimer's Disease Neuroimaging I. Manifold regularized multitask feature learning for multimodality disease classification. Hum Brain Mapp. 2015;36(2):489–507.
16. Khazaee A, Ebrahimzadeh A, Babajani-Feremi A. Identifying patients with Alzheimer's disease using resting-state fMRI and graph theory. Clin Neurophysiol. 2015;126(11):2132–41.
17. Liu M, Zhang D, Shen D, Alzheimer's Disease Neuroimaging I. View-centralized multi-atlas classification for Alzheimer's disease diagnosis. Hum Brain Mapp. 2015;36(5):1847–65.
18. Liu S, Liu S, Cai W, Che H, Pujol S, Kikinis R, et al. Multimodal neuroimaging feature learning for multiclass diagnosis of Alzheimer's disease. IEEE Trans Biomed Eng. 2015;62(4):1132–40.
19. Moradi E, Pepe A, Gaser C, Huttunen H, Tohka J, Alzheimer's Disease Neuroimaging I. Machine learning framework for early MRI-based Alzheimer's conversion prediction in MCI subjects. Neuroimage. 2015;104:398–412.
20. Xu L, Wu X, Chen K, Yao L. Multi-modality sparse representation-based classification for Alzheimer's disease and mild cognitive impairment. Comput Methods Progr Biomed. 2015;122(2):182–90.
21. Zhu X, Suk HI, Zhu Y, Thung KH, Wu G, Shen D. Multi-view classification for identification of Alzheimer's disease. Mach Learn Med Imaging. 2015;9352:255–62.
22. Cattell L, Platsch G, Pfeiffer R, Declerck J, Schnabel JA, Hutton C, et al. Classification of amyloid status using machine learning with histograms of oriented 3D gradients. Neuroimage Clin. 2016;12:990–1003.
23. Hu C, Sepulcre J, Johnson KA, Fakhri GE, Lu YM, Li Q. Matched signal detection on graphs: theory and application to brain imaging data classification. Neuroimage. 2016;125:587–600.
24. Khazaee A, Ebrahimzadeh A, Babajani-Feremi A. Application of advanced machine learning methods on resting-state fMRI network for identification of mild cognitive impairment and Alzheimer's disease. Brain Imaging Behav. 2016;10(3):799–817.
25. Liu M, Zhang D, Shen D. Relationship induced multi-template learning for diagnosis of Alzheimer's disease and mild cognitive impairment. IEEE Trans Med Imaging. 2016;35(6):1463–74.
26. Ni H, Zhou L, Ning X, Wang L, Alzheimer's Disease Neuroimaging I. Exploring multifractal-based features for mild Alzheimer's disease classification. Magn Reson Med. 2016;76(1):259–69.
27. Suk HI, Wee CY, Lee SW, Shen D. State-space model with deep learning for functional dynamics estimation in resting-state fMRI. Neuroimage. 2016;129:292–307.
28. Yu G, Liu Y, Shen D. Graph-guided joint prediction of class label and clinical scores for the Alzheimer's disease. Brain Struct Funct. 2016;221(7):3787–801.
29. Zu C, Jie B, Liu M, Chen S, Shen D, Zhang D, et al. Label-aligned multi-task feature learning for multimodal classification of Alzheimer's disease and mild cognitive impairment. Brain Imaging Behav. 2016;10(4):1148–59.
30. An L, Adeli E, Liu M, Zhang J, Lee SW, Shen D. A hierarchical feature and sample selection framework and its application for Alzheimer's disease diagnosis. Sci Rep. 2017;7:45269.
31. Beheshti I, Demirel H, Matsuda H, Alzheimer's Disease Neuroimaging I. Classification of Alzheimer's disease and prediction of mild cognitive impairment-to-Alzheimer's conversion from structural magnetic resource imaging using feature ranking and a genetic algorithm. Comput Biol Med. 2017;83:109–19.
32. Chen X, Zhang H, Zhang L, Shen C, Lee SW, Shen D. Extraction of dynamic functional connectivity from brain grey matter and white matter for MCI classification. Hum Brain Mapp. 2017;38(10):5019–34.
33. Doan NT, Engvig A, Zaske K, Persson K, Lund MJ, Kaufmann T, et al. Distinguishing early and late brain aging from the

Alzheimer's disease spectrum: consistent morphological patterns across independent samples. Neuroimage. 2017;158:282–95.
34. Glozman T, Solomon J, Pestilli F, Guibas L, Alzheimer's Disease Neuroimaging I. Shape-attributes of brain structures as biomarkers for Alzheimer's disease. J Alzheimers Dis. 2017;56(1):287–95.
35. Guan H, Liu T, Jiang J, Tao D, Zhang J, Niu H, et al. Classifying MCI subtypes in community-dwelling elderly using cross-sectional and longitudinal MRI-Based biomarkers. Front Aging Neurosci. 2017;9:309.
36. Guo H, Zhang F, Chen J, Xu Y, Xiang J. Machine learning classification combining multiple features of a hyper-network of fMRI data in Alzheimer's disease. Front Neurosci. 2017;11:615.
37. Hojjati SH, Ebrahimzadeh A, Khazaee A, Babajani-Feremi A, Alzheimer's Disease Neuroimaging I. Predicting conversion from MCI to AD using resting-state fMRI, graph theoretical approach and SVM. J Neurosci Methods. 2017;282:69–80.
38. Kawaguchi A, Yamashita F, Alzheimer's Disease Neuroimaging I. Supervised multiblock sparse multivariable analysis with application to multimodal brain imaging genetics. Biostatistics. 2017;18(4):651–65.
39. Khazaee A, Ebrahimzadeh A, Babajani-Feremi A, Alzheimer's Disease Neuroimaging I. Classification of patients with MCI and AD from healthy controls using directed graph measures of resting-state fMRI. Behav Brain Res. 2017;322(Pt B):339–50.
40. Lama RK, Gwak J, Park JS, Lee SW. Diagnosis of Alzheimer's disease based on structural MRI images using a regularized extreme learning machine and PCA features. J Healthc Eng. 2017;2017:5485080.
41. Li Q, Wu X, Xu L, Chen K, Yao L, Li R. Multi-modal discriminative dictionary learning for Alzheimer's disease and mild cognitive impairment. Comput Methods Progr Biomed. 2017;150:1–8.
42. Long X, Chen L, Jiang C, Zhang L, Alzheimer's Disease Neuroimaging I. Prediction and classification of Alzheimer disease based on quantification of MRI deformation. PLoS One. 2017;12(3):e0173372.
43. Min J, Moon WJ, Jeon JY, Choi JW, Moon YS, Han SH. Diagnostic efficacy of structural MRI in patients with mild-to-moderate Alzheimer disease: automated volumetric assessment versus visual assessment. AJR Am J Roentgenol. 2017;208(3):617–23.
44. Proitsi P, Kim M, Whiley L, Simmons A, Sattlecker M, Velayudhan L, et al. Association of blood lipids with Alzheimer's disease: a comprehensive lipidomics analysis. Alzheimers Dement. 2017;13(2):140–51.
45. Sorensen L, Igel C, Pai A, Balas I, Anker C, Lillholm M, et al. Differential diagnosis of mild cognitive impairment and Alzheimer's disease using structural MRI cortical thickness, hippocampal shape, hippocampal texture, and volumetry. Neuroimage Clin. 2017;13:470–82.
46. Suk HI, Lee SW, Shen D, Alzheimer's Disease Neuroimaging I. Deep ensemble learning of sparse regression models for brain disease diagnosis. Med Image Anal. 2017;37:101–13.
47. Youssofzadeh V, McGuinness B, Maguire LP, Wong-Lin K. Multi-Kernel learning with Dartel improves combined MRI-PET classification of Alzheimer's disease in AIBL data: group and individual analyses. Front Hum Neurosci. 2017;11:380.
48. Zhu X, Suk HI, Lee SW, Shen D. Discriminative self-representation sparse regression for neuroimaging-based Alzheimer's disease diagnosis. Brain Imaging Behav. 2017. https://doi.org/10.1007/s11682-017-9731-x.
49. Zhu X, Suk HI, Wang L, Lee SW, Shen D, Alzheimer's Disease Neuroimaging I. A novel relational regularization feature selection method for joint regression and classification in AD diagnosis. Med Image Anal. 2017;38:205–14.
50. Amoroso N, Rocca M, Bellotti R, Fanizzi A, Monaco A, Tangaro S, et al. Alzheimer's disease diagnosis based on the hippocampal unified multi-atlas network (HUMAN) algorithm. Biomed Eng Online. 2018;17(1):6.
51. Choi H, Jin KH, Alzheimer's Disease Neuroimaging I. Predicting cognitive decline with deep learning of brain metabolism and amyloid imaging. Behav Brain Res. 2018;344:103–9.
52. Garali I, Adel M, Bourennane S, Guedj E. Histogram-Based features selection and volume of interest ranking for brain PET image classification. IEEE J Transl Eng Health Med. 2018;6:2100212.
53. Kim J, Lee B. Identification of Alzheimer's disease and mild cognitive impairment using multimodal sparse hierarchical extreme learning machine. Hum Brain Mapp. 2018. https://doi.org/10.1002/hbm.24207.
54. Liu M, Cheng D, Wang K, Wang Y, Alzheimer's Disease Neuroimaging I. Multi-modality cascaded convolutional neural networks for Alzheimer's disease diagnosis. Neuroinformatics. 2018;16(3–4):295–308.
55. Rondina JM, Ferreira LK, de Souza Duran FL, Kubo R, Ono CR, Leite CC, et al. Selecting the most relevant brain regions to discriminate Alzheimer's disease patients from healthy controls using multiple kernel learning: a comparison across functional and structural imaging modalities and atlases. Neuroimage Clin. 2018;17:628–41.
56. Salvatore C, Castiglioni I. A wrapped multi-label classifier for the automatic diagnosis and prognosis of Alzheimer's disease. J Neurosci Methods. 2018;302:58–65.
57. Sun Z, Qiao Y, Lelieveldt BPF, Staring M, Alzheimer's Disease NeuroImaging I. Integrating spatial-anatomical regularization and structure sparsity into SVM: improving interpretation of Alzheimer's disease classification. Neuroimage. 2018;178:445–60.
58. Wang SH, Phillips P, Sui Y, Liu B, Yang M, Cheng H. Classification of Alzheimer's disease based on eight-layer convolutional neural network with leaky rectified linear unit and max pooling. J Med Syst. 2018;42(5):85.
59. Chen Y, Sha M, Zhao X, Ma J, Ni H, Gao W, et al. Automated detection of pathologic white matter alterations in Alzheimer's disease using combined diffusivity and kurtosis method. Psychiatry Res Neuroimaging. 2017;264:35–45.
60. Schouten TM, Koini M, Vos F, Seiler S, Rooij M, Lechner A, et al. Individual classification of Alzheimer's disease with diffusion magnetic resonance imaging. Neuroimage. 2017;152:476–81.
61. Sorensen L, Igel C, Liv Hansen N, Osler M, Lauritzen M, Rostrup E, et al. Early detection of Alzheimer's disease using MRI hippocampal texture. Hum Brain Mapp. 2016;37(3):1148–61.
62. Varol E, Sotiras A, Davatzikos C, Alzheimer's Disease Neuroimaging I. HYDRA: revealing heterogeneity of imaging and genetic patterns through a multiple max-margin discriminative analysis framework. Neuroimage. 2017;145(Pt B):346–64.
63. Cai K, Xu H, Guan H, Zhu W, Jiang J, Cui Y, et al. Identification of early-stage Alzheimer's disease using sulcal morphology and other common neuroimaging indices. PLoS One. 2017;12(1):e0170875.
64. Jie B, Liu M, Liu J, Zhang D, Shen D. Temporally constrained group sparse learning for longitudinal data analysis in Alzheimer's disease. IEEE Trans Biomed Eng. 2017;64(1):238–49.
65. Zhou M, Scott J, Chaudhury B, Hall L, Goldgof D, Yeom KW, Iv M, Ou Y, Kalpathy-Cramer J, Napel S, Gillies R, Gevaert O, Gatenby R. Radiomics in brain tumor: image assessment, quantitative feature descriptors, and machine-learning approaches. AJNR Am J Neuroradiol. 2018;39:208–16.

66. Imani F, Boada FE, Lieberman FS, Davis DK, Mountz JM. Molecular and metabolic pattern classification for detection of brain glioma progression. Eur J Radiol. 2014;83(2):e100–5.
67. Nachimuthu DS, Baladhandapani A. Multidimensional texture characterization: on analysis for brain tumor tissues using MRS and MRI. J Digit Imaging. 2014;27(4):496–506.
68. Sunwoo L, Kim YJ, Choi SH, Kim KG, Kang JH, Kang Y, et al. Computer-aided detection of brain metastasis on 3D MR imaging: observer performance study. PLoS One. 2017;12(6):e0178265.
69. Wu W, Chen AY, Zhao L, Corso JJ. Brain tumor detection and segmentation in a CRF (conditional random fields) framework with pixel-pairwise affinity and superpixel-level features. Int J Comput Assist Radiol Surg. 2014;9(2):241–53.
70. Fathi Kazerooni A, Mohseni M, Rezaei S, Bakhshandehpour G, Saligheh Rad H. Multi-parametric (ADC/PWI/T2-w) image fusion approach for accurate semi-automatic segmentation of tumorous regions in glioblastoma multiforme. MAGMA. 2015;28(1):13–22.
71. Szwarc P, Kawa J, Rudzki M, Pietka E. Automatic brain tumour detection and neovasculature assessment with multiseries MRI analysis. Comput Med Imaging Graph. 2015;46(Pt 2):178–90.
72. Havaei M, Davy A, Warde-Farley D, Biard A, Courville A, Bengio Y, et al. Brain tumor segmentation with deep neural networks. Med Image Anal. 2017;35:18–31.
73. Li Y, Liu X, Wei F, Sima DM, Van Cauter S, Himmelreich U, et al. An advanced MRI and MRSI data fusion scheme for enhancing unsupervised brain tumor differentiation. Comput Biol Med. 2017;81:121–9.
74. Sauwen N, Acou M, Sima DM, Veraart J, Maes F, Himmelreich U, et al. Semi-automated brain tumor segmentation on multi-parametric MRI using regularized non-negative matrix factorization. BMC Med Imaging. 2017;17(1):29.
75. AlBadawy EA, Saha A, Mazurowski MA. Deep learning for segmentation of brain tumors: Impact of cross-institutional training and testing. Med Phys. 2018;45(3):1150–8.
76. Blanc-Durand P, Van Der Gucht A, Schaefer N, Itti E, Prior JO. Automatic lesion detection and segmentation of 18F-FET PET in gliomas: a full 3D U-Net convolutional neural network study. PLoS One. 2018;13(4):e0195798.
77. Soltaninejad M, Yang G, Lambrou T, Allinson N, Jones TL, Barrick TR, et al. Supervised learning based multimodal MRI brain tumour segmentation using texture features from supervoxels. Comput Methods Progr Biomed. 2018;157:69–84.
78. Zhao Z, Yang G, Lin Y, Pang H, Wang M. Automated glioma detection and segmentation using graphical models. PLoS One. 2018;13(8):e0200745.
79. Inano R, Oishi N, Kunieda T, Arakawa Y, Yamao Y, Shibata S, et al. Voxel-based clustered imaging by multiparameter diffusion tensor images for glioma grading. Neuroimage Clin. 2014;5:396–407.
80. Fetit AE, Novak J, Peet AC, Arvanitits TN. Three-dimensional textural features of conventional MRI improve diagnostic classification of childhood brain tumours. NMR Biomed. 2015;28(9):1174–84.
81. Hu LS, Ning S, Eschbacher JM, Gaw N, Dueck AC, Smith KA, et al. Multi-Parametric MRI and texture analysis to visualize spatial histologic heterogeneity and tumor extent in glioblastoma. PLoS One. 2015;10(11):e0141506.
82. Tsolaki E, Svolos P, Kousi E, Kapsalaki E, Fezoulidis I, Fountas K, et al. Fast spectroscopic multiple analysis (FASMA) for brain tumor classification: a clinical decision support system utilizing multi-parametric 3T MR data. Int J Comput Assist Radiol Surg. 2015;10(7):1149–66.
83. Li-Chun Hsieh K, Chen CY, Lo CM. Quantitative glioma grading using transformed gray-scale invariant textures of MRI. Comput Biol Med. 2017;83:102–8.
84. Zhang X, Yan LF, Hu YC, Li G, Yang Y, Han Y, et al. Optimizing a machine learning based glioma grading system using multi-parametric MRI histogram and texture features. Oncotarget. 2017;8(29):47816–30.
85. De Looze C, Beausang A, Cryan J, Loftus T, Buckley PG, Farrell M, et al. Machine learning: a useful radiological adjunct in determination of a newly diagnosed glioma's grade and IDH status. J Neurooncol. 2018;139(2):491–9.
86. Fetit AE, Novak J, Rodriguez D, Auer DP, Clark CA, Grundy RG, et al. Radiomics in paediatric neuro-oncology: a multicentre study on MRI texture analysis. NMR Biomed. 2018. https://doi.org/10.1002/nbm.3781.
87. Shofty B, Artzi M, Ben Bashat D, Liberman G, Haim O, Kashanian A, et al. MRI radiomics analysis of molecular alterations in low-grade gliomas. Int J Comput Assist Radiol Surg. 2018;13(4):563–71.
88. Zarinabad N, Abernethy LJ, Avula S, Davies NP, Rodriguez Gutierrez D, Jaspan T, et al. Application of pattern recognition techniques for classification of pediatric brain tumors by in vivo 3T (1) H-MR spectroscopy-A multi-center study. Magn Reson Med. 2018;79(4):2359–66.
89. Qian X, Tan H, Zhang J, Zhao W, Chan MD, Zhou X. Stratification of pseudoprogression and true progression of glioblastoma multiform based on longitudinal diffusion tensor imaging without segmentation. Med Phys. 2016;43(11):5889.
90. Zhang J, Yu H, Qian X, Liu K, Tan H, Yang T, et al. Pseudo progression identification of glioblastoma with dictionary learning. Comput Biol Med. 2016;73:94–101.
91. Emblem KE, Due-Tonnessen P, Hald JK, Bjornerud A, Pinho MC, Scheie D, et al. Machine learning in preoperative glioma MRI: survival associations by perfusion-based support vector machine outperforms traditional MRI. J Magn Reson Imaging. 2014;40(1):47–54.
92. Emblem KE, Pinho MC, Zollner FG, Due-Tonnessen P, Hald JK, Schad LR, et al. A generic support vector machine model for preoperative glioma survival associations. Radiology. 2015;275(1):228–34.
93. Akbari H, Macyszyn L, Da X, Bilello M, Wolf RL, Martinez-Lage M, et al. Imaging surrogates of infiltration obtained via multiparametric imaging pattern analysis predict subsequent location of recurrence of glioblastoma. Neurosurgery. 2016;78(4):572–80.
94. Chang K, Zhang B, Guo X, Zong M, Rahman R, Sanchez D, et al. Multimodal imaging patterns predict survival in recurrent glioblastoma patients treated with bevacizumab. Neuro Oncol. 2016;18(12):1680–7.
95. Korfiatis P, Kline TL, Coufalova L, Lachance DH, Parney IF, Carter RE, et al. MRI texture features as biomarkers to predict MGMT methylation status in glioblastomas. Med Phys. 2016;43(6):2835–44.
96. Macyszyn L, Akbari H, Pisapia JM, Da X, Attiah M, Pigrish V, et al. Imaging patterns predict patient survival and molecular subtype in glioblastoma via machine learning techniques. Neuro Oncol. 2016;18(3):417–25.
97. Akkus Z, Ali I, Sedlar J, Agrawal JP, Parney IF, Giannini C, et al. Predicting deletion of chromosomal arms 1p/19q in low-grade gliomas from MR images using machine intelligence. J Digit Imaging. 2017;30(4):469–76.
98. Chen L, Zhang H, Thung KH, Liu L, Lu J, Wu J, et al. Multi-label inductive matrix completion for joint MGMT and IDH1 status prediction for glioma patients. Med Image Comput Comput Assist Interv. 2017;10434:450–8.

99. Zhang B, Chang K, Ramkissoon S, Tanguturi S, Bi WL, Reardon DA, et al. Multimodal MRI features predict isocitrate dehydrogenase genotype in high-grade gliomas. Neuro Oncol. 2017;19(1):109–17.
100. Zhou M, Chaudhury B, Hall LO, Goldgof DB, Gillies RJ, Gatenby RA. Identifying spatial imaging biomarkers of glioblastoma multiforme for survival group prediction. J Magn Reson Imaging. 2017;46(1):115–23.
101. Li Y, Qian Z, Xu K, Wang K, Fan X, Li S, et al. MRI features predict p53 status in lower-grade gliomas via a machine-learning approach. Neuroimage Clin. 2018;17:306–11.
102. Papp L, Potsch N, Grahovac M, Schmidbauer V, Woehrer A, Preusser M, et al. Glioma survival prediction with combined analysis of in vivo (11)C-MET PET features, ex vivo features, and patient features by supervised machine learning. J Nucl Med. 2018;59(6):892–9.
103. Anticevic A, Cole MW, Repovs G, Murray JD, Brumbaugh MS, Winkler AM, et al. Characterizing thalamo-cortical disturbances in schizophrenia and bipolar illness. Cereb Cortex. 2014;24(12):3116–30.
104. Bleich-Cohen M, Jamshy S, Sharon H, Weizman R, Intrator N, Poyurovsky M, et al. Machine learning fMRI classifier delineates subgroups of schizophrenia patients. Schizophr Res. 2014;160(1–3):196–200.
105. Castro E, Gupta CN, Martinez-Ramon M, Calhoun VD, Arbabshirani MR, Turner J. Identification of patterns of gray matter abnormalities in schizophrenia using source-based morphometry and bagging. Conf Proc IEEE Eng Med Biol Soc. 2014;2014:1513–6.
106. Schnack HG, Nieuwenhuis M, van Haren NE, Abramovic L, Scheewe TW, Brouwer RM, et al. Can structural MRI aid in clinical classification? A machine learning study in two independent samples of patients with schizophrenia, bipolar disorder and healthy subjects. Neuroimage. 2014;84:299–306.
107. Cheng H, Newman S, Goni J, Kent JS, Howell J, Bolbecker A, et al. Nodal centrality of functional network in the differentiation of schizophrenia. Schizophr Res. 2015;168(1–2):345–52.
108. Chyzhyk D, Grana M, Ongur D, Shinn AK. Discrimination of schizophrenia auditory hallucinators by machine learning of resting-state functional MRI. Int J Neural Syst. 2015;25(3):1550007.
109. Chyzhyk D, Savio A, Grana M. Computer aided diagnosis of schizophrenia on resting state fMRI data by ensembles of ELM. Neural Netw. 2015;68:23–33.
110. Koch SP, Hagele C, Haynes JD, Heinz A, Schlagenhauf F, Sterzer P. Diagnostic classification of schizophrenia patients on the basis of regional reward-related FMRI signal patterns. PLoS One. 2015;10(3):e0119089.
111. Chu WL, Huang MW, Jian BL, Hsu CY, Cheng KS. A correlative classification study of schizophrenic patients with results of clinical evaluation and structural magnetic resonance images. Behav Neurol. 2016;2016:7849526.
112. Kim J, Calhoun VD, Shim E, Lee JH. Deep neural network with weight sparsity control and pre-training extracts hierarchical features and enhances classification performance: evidence from whole-brain resting-state functional connectivity patterns of schizophrenia. Neuroimage. 2016;124(Pt A):127–46.
113. Lu X, Yang Y, Wu F, Gao M, Xu Y, Zhang Y, et al. Discriminative analysis of schizophrenia using support vector machine and recursive feature elimination on structural MRI images. Medicine (Baltimore). 2016;95(30):e3973.
114. Pinaya WH, Gadelha A, Doyle OM, Noto C, Zugman A, Cordeiro Q, et al. Using deep belief network modelling to characterize differences in brain morphometry in schizophrenia. Sci Rep. 2016;6:38897.
115. Pergola G, Trizio S, Di Carlo P, Taurisano P, Mancini M, Amoroso N, et al. Grey matter volume patterns in thalamic nuclei are associated with familial risk for schizophrenia. Schizophr Res. 2017;180:13–20.
116. Plaschke RN, Cieslik EC, Muller VI, Hoffstaedter F, Plachti A, Varikuti DP, et al. On the integrity of functional brain networks in schizophrenia, Parkinson's disease, and advanced age: evidence from connectivity-based single-subject classification. Hum Brain Mapp. 2017;38(12):5845–58.
117. Qureshi MNI, Oh J, Cho D, Jo HJ, Lee B. Multimodal discrimination of schizophrenia using hybrid weighted feature concatenation of brain functional connectivity and anatomical features with an extreme learning machine. Front Neuroinform. 2017;11:59.
118. Skatun KC, Kaufmann T, Doan NT, Alnaes D, Cordova-Palomera A, Jonsson EG, et al. Consistent functional connectivity alterations in schizophrenia spectrum disorder: a multisite study. Schizophr Bull. 2017;43(4):914–24.
119. Zarogianni E, Storkey AJ, Johnstone EC, Owens DG, Lawrie SM. Improved individualized prediction of schizophrenia in subjects at familial high risk, based on neuroanatomical data, schizotypal and neurocognitive features. Schizophr Res. 2017;181:6–12.
120. Juneja A, Rana B, Agrawal RK. A novel fuzzy rough selection of non-linearly extracted features for schizophrenia diagnosis using fMRI. Comput Methods Progr Biomed. 2018;155:139–52.
121. Mikolas P, Hlinka J, Skoch A, Pitra Z, Frodl T, Spaniel F, et al. Machine learning classification of first-episode schizophrenia spectrum disorders and controls using whole brain white matter fractional anisotropy. BMC Psychiatry. 2018;18(1):97.
122. Orban P, Dansereau C, Desbois L, Mongeau-Perusse V, Giguere CE, Nguyen H, et al. Multisite generalizability of schizophrenia diagnosis classification based on functional brain connectivity. Schizophr Res. 2018;192:167–71.
123. Zeng LL, Wang H, Hu P, Yang B, Pu W, Shen H, et al. Multi-site diagnostic classification of schizophrenia using discriminant deep learning with functional connectivity MRI. EBioMedicine. 2018;30:74–85.
124. Papakostas GI. Managing partial response or nonresponse: switching, augmentation, and combination strategies for major depressive disorder. J Clin Psychol. 2009;70(Suppl. 6):16–25.
125. Cao L, Guo S, Xue Z, Hu Y, Liu H, Mwansisya TE, et al. Aberrant functional connectivity for diagnosis of major depressive disorder: a discriminant analysis. Psychiatry Clin Neurosci. 2014;68(2):110–9.
126. Qin J, Wei M, Liu H, Chen J, Yan R, Hua L, et al. Abnormal hubs of white matter networks in the frontal-parieto circuit contribute to depression discrimination via pattern classification. Magn Reson Imaging. 2014;32(10):1314–20.
127. Zeng LL, Shen H, Liu L, Hu D. Unsupervised classification of major depression using functional connectivity MRI. Hum Brain Mapp. 2014;35(4):1630–41.
128. Lueken U, Straube B, Yang Y, Hahn T, Beesdo-Baum K, Wittchen HU, et al. Separating depressive comorbidity from panic disorder: a combined functional magnetic resonance imaging and machine learning approach. J Affect Disord. 2015;184:182–92.
129. Qin J, Wei M, Liu H, Chen J, Yan R, Yao Z, et al. Altered anatomical patterns of depression in relation to antidepressant treatment: evidence from a pattern recognition analysis on the topological organization of brain networks. J Affect Disord. 2015;180:129–37.
130. Sato JR, Moll J, Green S, Deakin JF, Thomaz CE, Zahn R. Machine learning algorithm accurately detects fMRI signature of vulnerability to major depression. Psychiatry Res. 2015;233(2):289–91.
131. Shimizu Y, Yoshimoto J, Toki S, Takamura M, Yoshimura S, Okamoto Y, et al. Toward probabilistic diagnosis and

understanding of depression based on functional MRI data analysis with logistic group LASSO. PLoS One. 2015;10(5):e0123524.
132. Wu MJ, Wu HE, Mwangi B, Sanches M, Selvaraj S, Zunta-Soares GB, et al. Prediction of pediatric unipolar depression using multiple neuromorphometric measurements: a pattern classification approach. J Psychiatr Res. 2015;62:84–91.
133. Ramasubbu R, Brown MR, Cortese F, Gaxiola I, Goodyear B, Greenshaw AJ, et al. Accuracy of automated classification of major depressive disorder as a function of symptom severity. Neuroimage Clin. 2016;12:320–31.
134. Bhaumik R, Jenkins LM, Gowins JR, Jacobs RH, Barba A, Bhaumik DK, et al. Multivariate pattern analysis strategies in detection of remitted major depressive disorder using resting state functional connectivity. Neuroimage Clin. 2017;16:390–8.
135. Kautzky A, James GM, Philippe C, Baldinger-Melich P, Kraus C, Kranz GS, et al. The influence of the rs6295 gene polymorphism on serotonin-1A receptor distribution investigated with PET in patients with major depression applying machine learning. Transl Psychiatry. 2017;7(6):e1150.
136. Schnyer DM, Clasen PC, Gonzalez C, Beevers CG. Evaluating the diagnostic utility of applying a machine learning algorithm to diffusion tensor MRI measures in individuals with major depressive disorder. Psychiatry Res Neuroimaging. 2017;264:1–9.
137. Wang J, Wei Q, Bai T, Zhou X, Sun H, Becker B, et al. Electroconvulsive therapy selectively enhanced feedforward connectivity from fusiform face area to amygdala in major depressive disorder. Soc Cogn Affect Neurosci. 2017;12(12):1983–92.
138. Deng F, Wang Y, Huang H, Niu M, Zhong S, Zhao L, et al. Abnormal segments of right uncinate fasciculus and left anterior thalamic radiation in major and bipolar depression. Prog Neuropsychopharmacol Biol Psychiatry. 2018;81:340–9.
139. Milak MS, Pantazatos S, Rashid R, Zanderigo F, DeLorenzo C, Hesselgrave N, et al. Higher 5-HT1A autoreceptor binding as an endophenotype for major depressive disorder identified in high risk offspring—a pilot study. Psychiatry Res Neuroimaging. 2018;276:15–23.
140. Foland-Ross LC, Sacchet MD, Prasad G, Gilbert B, Thompson PM, Gotlib IH. Cortical thickness predicts the first onset of major depression in adolescence. Int J Dev Neurosci. 2015;46:125–31.
141. Johnston BA, Steele JD, Tolomeo S, Christmas D, Matthews K. Structural MRI-based predictions in patients with treatment-refractory depression (TRD). PLoS One. 2015;10(7):e0132958.
142. Patel MJ, Andreescu C, Price JC, Edelman KL, Reynolds CF 3rd, Aizenstein HJ. Machine learning approaches for integrating clinical and imaging features in late-life depression classification and response prediction. Int J Geriatr Psychiatry. 2015;30(10):1056–67.
143. Redlich R, Opel N, Grotegerd D, Dohm K, Zaremba D, Burger C, et al. Prediction of individual response to electroconvulsive therapy via machine learning on structural magnetic resonance imaging data. JAMA Psychiatry. 2016;73(6):557–64.
144. Yoshida K, Shimizu Y, Yoshimoto J, Takamura M, Okada G, Okamoto Y, et al. Prediction of clinical depression scores and detection of changes in whole-brain using resting-state functional MRI data with partial least squares regression. PLoS One. 2017;12(7):e0179638.
145. Adeli E, Shi F, An L, Wee CY, Wu G, Wang T, et al. Joint feature-sample selection and robust diagnosis of Parkinson's disease from MRI data. Neuroimage. 2016;141:206–19.
146. Choi H, Ha S, Im HJ, Paek SH, Lee DS. Refining diagnosis of Parkinson's disease with deep learning-based interpretation of dopamine transporter imaging. Neuroimage Clin. 2017;16:586–94.
147. Peng B, Wang S, Zhou Z, Liu Y, Tong B, Zhang T, et al. A multilevel-ROI-features-based machine learning method for detection of morphometric biomarkers in Parkinson's disease. Neurosci Lett. 2017;651:88–94.
148. Amoroso N, La Rocca M, Monaco A, Bellotti R, Tangaro S. Complex networks reveal early MRI markers of Parkinson's disease. Med Image Anal. 2018;48:12–24.
149. Castillo-Barnes D, Ramirez J, Segovia F, Martinez-Murcia FJ, Salas-Gonzalez D, Gorriz JM. Robust ensemble classification methodology for I123-ioflupane SPECT images and multiple heterogeneous biomarkers in the diagnosis of Parkinson's disease. Front Neuroinform. 2018;12:53.
150. Oliveira FPM, Faria DB, Costa DC, Castelo-Branco M, Tavares J. Extraction, selection and comparison of features for an effective automated computer-aided diagnosis of Parkinson's disease based on [(123)I]FP-CIT SPECT images. Eur J Nucl Med Mol Imaging. 2018;45(6):1052–62.
151. Salvatore C, Cerasa A, Castiglioni I, Gallivanone F, Augimeri A, Lopez M, et al. Machine learning on brain MRI data for differential diagnosis of Parkinson's disease and progressive supranuclear palsy. J Neurosci Methods. 2014;222:230–7.
152. Hirschauer TJ, Adeli H, Buford JA. Computer-Aided diagnosis of Parkinson's disease using enhanced probabilistic neural network. J Med Syst. 2015;39(11):179.
153. Huertas-Fernandez I, Garcia-Gomez FJ, Garcia-Solis D, Benitez-Rivero S, Marin-Oyaga VA, Jesus S, et al. Machine learning models for the differential diagnosis of vascular parkinsonism and Parkinson's disease using [(123)I]FP-CIT SPECT. Eur J Nucl Med Mol Imaging. 2015;42(1):112–9.
154. Singh G, Samavedham L. Unsupervised learning based feature extraction for differential diagnosis of neurodegenerative diseases: a case study on early-stage diagnosis of Parkinson disease. J Neurosci Methods. 2015;256:30–40.
155. Liu L, Wang Q, Adeli E, Zhang L, Zhang H, Shen D. Feature selection based on iterative canonical correlation analysis for automatic diagnosis of Parkinson's disease. Med Image Comput Comput Assist Interv. 2016;9901:1–8.
156. Du G, Lewis MM, Kanekar S, Sterling NW, He L, Kong L, et al. Combined diffusion tensor imaging and apparent transverse relaxation rate differentiate Parkinson disease and atypical parkinsonism. AJNR Am J Neuroradiol. 2017;38(5):966–72.
157. Ye Z, Rae CL, Nombela C, Ham T, Rittman T, Jones PS, et al. Predicting beneficial effects of atomoxetine and citalopram on response inhibition in Parkinson's disease with clinical and neuroimaging measures. Hum Brain Mapp. 2016;37(3):1026–37.
158. ADHD200 - international neuroimaging data-sharing initiative - NITRC. http://.fcon_1000.projects.nitrc.org/indi/adhd200. Accessed Oct 2018.
159. Qureshi MN, Min B, Jo HJ, Lee B. Multiclass classification for the differential diagnosis on the ADHD subtypes using recursive feature elimination and hierarchical extreme learning machine: structural MRI study. PLoS One. 2016;11(8):e0160697.
160. Qureshi MNI, Oh J, Min B, Jo HJ, Lee B. Multi-modal, multi-measure, and multi-class discrimination of ADHD with hierarchical feature extraction and extreme learning machine using structural and functional brain MRI. Front Hum Neurosci. 2017;11:157.
161. Tan L, Guo X, Ren S, Epstein JN, Lu LJ. A computational model for the automatic diagnosis of attention deficit hyperactivity disorder based on functional brain volume. Front Comput Neurosci. 2017;11:75.
162. Hart H, Chantiluke K, Cubillo AI, Smith AB, Simmons A, Brammer MJ, et al. Pattern classification of response inhibition in ADHD: toward the development of neurobiological markers for ADHD. Hum Brain Mapp. 2014;35(7):3083–94.
163. Johnston BA, Mwangi B, Matthews K, Coghill D, Konrad K, Steele JD. Brainstem abnormalities in attention deficit

hyperactivity disorder support high accuracy individual diagnostic classification. Hum Brain Mapp. 2014;35(10):5179–89.
164. Ghiassian S, Greiner R, Jin P, Brown MR. Using functional or structural magnetic resonance images and personal characteristic data to identify ADHD and autism. PLoS One. 2016;11(12):e0166934.
165. Xiao C, Bledsoe J, Wang S, Chaovalitwongse WA, Mehta S, Semrud-Clikeman M, et al. An integrated feature ranking and selection framework for ADHD characterization. Brain Inform. 2016;3(3):145–55.
166. Chaim-Avancini TM, Doshi J, Zanetti MV, Erus G, Silva MA, Duran FLS, et al. Neurobiological support to the diagnosis of ADHD in stimulant-naive adults: pattern recognition analyses of MRI data. Acta Psychiatr Scand. 2017;136(6):623–36.
167. Riaz A, Asad M, Alonso E, Slabaugh G. Fusion of fMRI and non-imaging data for ADHD classification. Comput Med Imaging Graph. 2018;65:115–28.
168. Sen B, Borle NC, Greiner R, Brown MRG. A general prediction model for the detection of ADHD and Autism using structural and functional MRI. PLoS One. 2018;13(4):e0194856.
169. Kim JW, Sharma V, Ryan ND. Predicting methylphenidate response in ADHD using machine learning approaches. Int J Neuropsychopharmacol. 2015;18(11):pyv052.
170. Matson JL, Rieske RD, Williams LW. The relationship between autism spectrum disorders and attention-deficit/hyperactivity disorder: an overview. Res Dev Disabil. 2013;34:2475–84.
171. Lord C, Risi S, Lambrecht L, Cook EH Jr, Leventhal BL, DiLavore PC, et al. The autism diagnostic observation schedule-generic: a standard measure of social and communication deficits associated with the spectrum of autism. J Autism Dev Disord. 2000;30:205–23.
172. Uddin LQ, Dajani DR, Voorhies W, Bednarz H, Kana RK. Progress and roadblocks in the search for brain-based biomarkers of autism and attention-deficit/hyperactivity disorder. Transl Psychiatry. 2017;7:e1218.
173. Just MA, Cherkassky VL, Buchweitz A, Keller TA, Mitchell TM. Identifying autism from neural representations of social interactions: neurocognitive markers of autism. PLoS One. 2014;9(12):e113879.
174. Chen CP, Keown CL, Jahedi A, Nair A, Pflieger ME, Bailey BA, et al. Diagnostic classification of intrinsic functional connectivity highlights somatosensory, default mode, and visual regions in autism. Neuroimage Clin. 2015;8:238–45.
175. Gori I, Giuliano A, Muratori F, Saviozzi I, Oliva P, Tancredi R, et al. Gray matter alterations in young children with autism spectrum disorders: comparing morphometry at the voxel and regional level. J Neuroimaging. 2015;25(6):866–74.
176. Iidaka T. Resting state functional magnetic resonance imaging and neural network classified autism and control. Cortex. 2015;63:55–67.
177. Plitt M, Barnes KA, Martin A. Functional connectivity classification of autism identifies highly predictive brain features but falls short of biomarker standards. Neuroimage Clin. 2015;7:359–66.
178. Jahedi A, Nasamran CA, Faires B, Fan J, Muller RA. Distributed intrinsic functional connectivity patterns predict diagnostic status in large autism cohort. Brain Connect. 2017;7(8):515–25.
179. Kam TE, Suk HI, Lee SW. Multiple functional networks modeling for autism spectrum disorder diagnosis. Hum Brain Mapp. 2017;38(11):5804–21.
180. Akhavan Aghdam M, Sharifi A, Pedram MM. Combination of rs-fMRI and sMRI data to discriminate autism spectrum disorders in young children using deep belief network. J Digit Imaging. 2018;31(6):895–903.
181. Bi XA, Wang Y, Shu Q, Sun Q, Xu Q. Classification of autism spectrum disorder using random support vector machine cluster. Front Genet. 2018;9:18.
182. Heinsfeld AS, Franco AR, Craddock RC, Buchweitz A, Meneguzzi F. Identification of autism spectrum disorder using deep learning and the ABIDE dataset. Neuroimage Clin. 2018;17:16–23.
183. Li H, Parikh NA, He L. A novel transfer learning approach to enhance deep neural network classification of brain functional connectomes. Front Neurosci. 2018;12:491.
184. Moradi E, Khundrakpam B, Lewis JD, Evans AC, Tohka J. Predicting symptom severity in autism spectrum disorder based on cortical thickness measures in agglomerative data. Neuroimage. 2017;144(Pt A):128–41.
185. Rudie JD, Colby JB, Salamon N. Machine learning classification of mesial temporal sclerosis in epilepsy patients. Epilepsy Res. 2015;117:63–9.
186. Hong SJ, Kim H, Schrader D, Bernasconi N, Bernhardt BC, Bernasconi A. Automated detection of cortical dysplasia type II in MRI-negative epilepsy. Neurology. 2014;83(1):48–55.
187. Kamiya K, Amemiya S, Suzuki Y, Kunii N, Kawai K, Mori H, et al. Machine learning of DTI structural brain connectomes for lateralization of temporal lobe epilepsy. Magn Reson Med Sci. 2016;15(1):121–9.
188. Del Gaizo J, Mofrad N, Jensen JH, Clark D, Glenn R, Helpern J, et al. Using machine learning to classify temporal lobe epilepsy based on diffusion MRI. Brain Behav. 2017;7(10):e00801.
189. Hong SJ, Bernhardt BC, Schrader DS, Bernasconi N, Bernasconi A. Whole-brain MRI phenotyping in dysplasia-related frontal lobe epilepsy. Neurology. 2016;86(7):643–50.
190. El Azami M, Hammers A, Jung J, Costes N, Bouet R, Lartizien C. Detection of lesions underlying intractable epilepsy on T1-weighted MRI as an outlier detection problem. PLoS One. 2016;11(9):e0161498.
191. Adler S, Wagstyl K, Gunny R, Ronan L, Carmichael D, Cross JH, et al. Novel surface features for automated detection of focal cortical dysplasias in paediatric epilepsy. Neuroimage Clin. 2017;14:18–27.
192. Bernhardt BC, Hong SJ, Bernasconi A, Bernasconi N. Magnetic resonance imaging pattern learning in temporal lobe epilepsy: classification and prognostics. Ann Neurol. 2015;77(3):436–46.
193. Munsell BC, Wee CY, Keller SS, Weber B, Elger C, da Silva LA, et al. Evaluation of machine learning algorithms for treatment outcome prediction in patients with epilepsy based on structural connectome data. Neuroimage. 2015;118:219–30.
194. Pustina D, Avants B, Sperling M, Gorniak R, He X, Doucet G, et al. Predicting the laterality of temporal lobe epilepsy from PET, MRI, and DTI: a multimodal study. Neuroimage Clin. 2015;9:20–31.
195. Zhong J, Chen DQ, Nantes JC, Holmes SA, Hodaie M, Koski L. Combined structural and functional patterns discriminating upper limb motor disability in multiple sclerosis using multivariate approaches. Brain Imaging Behav. 2017;11(3):754–68.
196. Yoo Y, Tang LYW, Brosch T, Li DKB, Kolind S, Vavasour I, et al. Deep learning of joint myelin and T1w MRI features in normal-appearing brain tissue to distinguish between multiple sclerosis patients and healthy controls. Neuroimage Clin. 2018;17:169–78.
197. Zurita M, Montalba C, Labbe T, Cruz JP, Dalboni da Rocha J, Tejos C, et al. Characterization of relapsing-remitting multiple sclerosis patients using support vector machine classifications of functional and diffusion MRI data. Neuroimage Clin. 2018;20:724–30.
198. Sacca V, Sarica A, Novellino F, Barone S, Tallarico T, Filippelli E, et al. Evaluation of machine learning algorithms performance

for the prediction of early multiple sclerosis from resting-state FMRI connectivity data. Brain Imaging Behav. 2018. https://doi.org/10.1007/s11682-018-9926-9.
199. Salem M, Cabezas M, Valverde S, Pareto D, Oliver A, Salvi J, et al. A supervised framework with intensity subtraction and deformation field features for the detection of new T2-w lesions in multiple sclerosis. Neuroimage Clin. 2018;17:607–15.
200. Zhao Y, Healy BC, Rotstein D, Guttmann CR, Bakshi R, Weiner HL, et al. Exploration of machine learning techniques in predicting multiple sclerosis disease course. PLoS One. 2017;12(4):e0174866.
201. Deshpande H, Maurel P, Barillot C. Classification of multiple sclerosis lesions using adaptive dictionary learning. Comput Med Imaging Graph. 2015;46(Pt 1):2–10.
202. Fartaria MJ, Bonnier G, Roche A, Kober T, Meuli R, Rotzinger D, et al. Automated detection of white matter and cortical lesions in early stages of multiple sclerosis. J Magn Reson Imaging. 2016;43(6):1445–54.
203. Lee Eun-Jae, Kim Yong-Hwan, Kim Namkug, Kanga Dong-Wha. Deep into the brain: artificial intelligence in stroke imaging. J Stroke. 2017;19(3):277–85.
204. Ashton EA, Takahashi C, Berg MJ, Goodman A, Totterman S, Ekholm S. Accuracy and reproducibility of manual and semi-automated quantification of MS lesions by MRI. J Magn Reson Imaging. 2003;17:300–8.
205. Bentley P, Ganesalingam J, Carlton Jones AL, Mahady K, Epton S, Rinne P, et al. Prediction of stroke thrombolysis outcome using CT brain machine learning. Neuroimage Clin. 2014;4:635640.
206. Kim BJ, Kim YH, Kim N, Kwon SU, Kim SJ, Kim JS, et al. Lesion location-based prediction of visual field improvement after cerebral infarction. PLoS One. 2015;10:e0143882.
207. Guberina N, Dietrich U, Radbruch A, Goebel J, Deuschl C, Ringelstein A, et al. Detection of early infarction signs with machine learning-based diagnosis by means of the Alberta Stroke Program Early CT score (ASPECTS) in the clinical routine. Neuroradiology. 2018;60(9):889–901.
208. Rehme AK, Volz LJ, Feis DL, Bomilcar-Focke I, Liebig T, Eickhoff SB, et al. Identifying neuroimaging markers of motor disability in acute stroke by machine learning techniques. Cereb Cortex. 2015;25(9):3046–56.
209. Asadi H, Dowling R, Yan B, Mitchell P. Machine learning for outcome prediction of acute ischemic stroke post intra-arterial therapy. PLoS One. 2014;9(2):e88225.
210. Bentley P, Ganesalingam J, Carlton Jones AL, Mahady K, Epton S, Rinne P, et al. Prediction of stroke thrombolysis outcome using CT brain machine learning. Neuroimage Clin. 2014;4:635–40.
211. Maier O, Schroder C, Forkert ND, Martinetz T, Handels H. Classifiers for ischemic stroke lesion segmentation: a comparison study. PLoS One. 2015;10(12):e0145118.
212. Griffis JC, Allendorfer JB, Szaflarski JP. Voxel-based Gaussian naive Bayes classification of ischemic stroke lesions in individual T1-weighted MRI scans. J Neurosci Methods. 2016;257:97–108.
213. Pustina D, Coslett HB, Turkeltaub PE, Tustison N, Schwartz MF, Avants B. Automated segmentation of chronic stroke lesions using LINDA: Lesion identification with neighborhood data analysis. Hum Brain Mapp. 2016;37(4):1405–21.
214. Douglas David B, Iv Michael, Douglas Pamela K, Ariana Anderson, Vos Sjoerd B, Bammer Roland, Zeineh Michael, Wintermark Max. Diffusion tensor imaging of TBI: potentials and challenges. Top Magn Reson Imaging. 2015;24(5):241–51.
215. Johansen-Berg H. Behavioural relevance of variation in white matter microstructure. Curr Opin Neurol. 2010;23(351–358):20581685.
216. Mitra J, Shen KK, Ghose S, Bourgeat P, Fripp J, Salvado O, et al. Statistical machine learning to identify traumatic brain injury (TBI) from structural disconnections of white matter networks. Neuroimage. 2016;129:247–59.
217. Peacock WFT, Van Meter TE, Mirshahi N, Ferber K, Gerwien R, Rao V, et al. Derivation of a three biomarker panel to improve diagnosis in patients with mild traumatic brain injury. Front Neurol. 2017;8:641.
218. Rangaprakash D, Deshpande G, Daniel TA, Goodman AM, Robinson JL, Salibi N, et al. Compromised hippocampus-striatum pathway as a potential imaging biomarker of mild-traumatic brain injury and posttraumatic stress disorder. Hum Brain Mapp. 2017;38(6):2843–64.
219. Vergara VM, Mayer AR, Damaraju E, Kiehl KA, Calhoun V. Detection of mild traumatic brain injury by machine learning classification using resting state functional network connectivity and fractional anisotropy. J Neurotrauma. 2017;34(5):1045–53.
220. Rangaprakash D, Dretsch MN, Venkataraman A, Katz JS, Denney TS Jr, Deshpande G. Identifying disease foci from static and dynamic effective connectivity networks: illustration in soldiers with trauma. Hum Brain Mapp. 2018;39(1):264–87.
221. Fagerholm ED, Hellyer PJ, Scott G, Leech R, Sharp DJ. Disconnection of network hubs and cognitive impairment after traumatic brain injury. Brain. 2015;138(Pt 6):1696–709.
222. Chong SL, Liu N, Barbier S, Ong ME. Predictive modeling in pediatric traumatic brain injury using machine learning. BMC Med Res Methodol. 2015;15:22.
223. OASIS brains - open access series of imaging studies. https://www.oasis-brains.org/. Accessed Oct 2018.
224. DZNE – longitudinal cognitive impairment and dementia study. https://www.dzne.de/en/research/studies/studien/delcode/. Accessed Oct 2018.
225. Seiler S, Schmidt H, Lechner A, Benke T. Driving cessation and dementia: results of the prospective registry on dementia in Austria PRODEM. PLoS One. 2012;7(12):1–6.
226. Ellis KA, Bush AI, Darby D, De Fazio D, Foster J, Hudson P, Lautenschlager NT, Lenzo N, Martins RN, Maruff P, et al. The Australian Imaging, Biomarkers and Lifestyle (AIBL) study of aging: methodology and baseline characteristics of 1112 individuals recruited for a longitudinal study of Alzheimer's disease. Int Psychogeriatr. 2009;21:672–87.
227. QIBA - quantitative imaging biomarkers alliance. https://www.linkedin.com/company/rsna-qiba. Accessed Oct 2018.
228. Shen Dinggang, Guorong Wu, Suk Heung-Il. Deep learning in medical image analysis. Annu Rev Biomed Eng. 2017;21(19):221–48.
229. Vieira S, Pinaya WHL, Mechelli A. Using deep learning to investigate the neuroimaging correlates of psychiatric and neurological disorders: methods and applications. Neurosci Biobehav Rev. 2017;74:58–75.